University of Dundee

Mechanisms mitigating problems with multiple kinetochores on one microtubule in early mitosis

Yue, Zuojun; Komoto, Shinya; Gierlinski, Marek; Pasquali, Debora; Kitamura, Etsushi; Tanaka, Tomoyuki U.

Mechanisms mitigating problems with multiple kinetochores on one microtubule in early mitosis

Zuojun Yue[1], Shinya Komoto[1,3,5], Marek Gierlinski[1,2,5], Debora Pasquali[1], Etsushi Kitamura[1,4] and Tomoyuki U. Tanaka[1]*

1. Centre for Gene Regulation and Expression, School of Life Sciences, University of Dundee, Dundee DD1 5EH, UK
2. Data Analysis Group, School of Life Sciences, University of Dundee, Dundee DD1 5EH, UK
3. Present address: Okinawa Institute of Science and Technology Graduate University, Onna, 904-0495 Japan
4. Present address: Institute of Molecular Embryology and Genetics, Kumamoto 860-0811 Japan
5. These authors contributed equally to this work.
*corresponding author

Key words: kinetochore, microtubule, kinetochore sliding, end-on attachment, early mitosis, budding yeast

Abstract

Proper chromosome segregation in mitosis relies on correct kinetochore interaction with spindle microtubules. In early mitosis, each kinetochore usually interacts with the lateral side of each microtubule and is subsequently tethered at the microtubule end. However, since eukaryotic cells carry multiple chromosomes, multiple kinetochores could occasionally interact with a single microtubule. The consequence of this is unknown. Here we find that, although two kinetochores (two pairs of sister kinetochores) can interact with the lateral side of one microtubule, only one kinetochore can form sustained attachment to the microtubule end in budding yeast. This leads to detachment of the other kinetochore from the microtubule end or its proximity. Intriguingly, in this context, kinetochore sliding along a microtubule towards a spindle pole delays and diminishes discernible kinetochore detachment. This effect expedites collection of the entire set of kinetochores to a spindle pole. We propose that cells are equipped with the kinetochore sliding mechanism to mitigate the problem with multiple kinetochores on one microtubule in early mitosis. (164 words)

Introduction

For proper chromosome segregation during mitosis, eukaryotic cells need to establish correct kinetochore–microtubule (KT–MT) interactions. This interaction is initiated and developed in a stepwise manner (Cheerambathur and Desai, 2014; Tanaka, 2010). During early stages of mitosis (prometaphase), a KT (a pair of sister KTs) makes initial contact with the MT lateral surface (lateral attachment; Figure 1A, left) (Rieder and Alexander, 1990; Tanaka et al., 2005). Once loaded on the MT lateral surface, the KT moves towards a spindle pole by sliding along the MT (Figure 1A, middle). This KT sliding is promoted by minus end-directed kinesin (kinesin-14) in budding yeast (Tanaka et al., 2007) and probably by KT-associated dynein (and kinesin-14) in vertebrates (Vorozhko et al., 2008; Yang et al., 2007). While the KT undergoes lateral sliding, the KT-associated MT depolymerizes at its distal plus end; in budding yeast, the speed of this depolymerization is higher than the speed of KT lateral sliding, resulting in the MT plus end often catching up with a KT attached to its lateral surface (Kitamura et al., 2007; Tanaka et al., 2007). In this event, the KT becomes tethered at the MT plus end (end-on attachment), and moves further towards a spindle pole as MT depolymerization continues at its plus end (end-on pulling; Figure 1A, right) (Maure et al., 2011; Shrestha and Draviam, 2013). Once KTs are collected on the mitotic spindle, sister KTs can efficiently bi-orient, i.e. interact with MTs extending from opposite spindle poles (Tanaka et al., 2002). All sister KTs must bi-orient prior to chromosome segregation at anaphase.

Poleward KT movement, either by sliding or end-on pulling, is especially crucial when KTs are located at some distance from the mitotic spindle. However, it is unknown why the majority of cells (including budding yeast and vertebrate cells) undergo both sliding and end-on pulling for poleward KT movement. In principle, to transport KTs to a spindle pole, end-on pulling should be sufficient and KT sliding should not be required; i.e. the KT could establish end-on attachment first and then could be transported towards the spindle by end-on pulling as the MT shrinks. In fact, some types of cells, such as fission yeast, undergo KT end-on pulling, but not KT sliding (Franco et al., 2007; Grishchuk and McIntosh, 2006). Is there, then, any advantage of KT sliding in the cells where this mechanism is present?

In both yeast and vertebrate cells, usually each KT (a pair of sister KTs) attaches to the lateral side of a single MT and becomes tethered at the MT end, as mentioned in the first paragraph; subsequently vertebrate KTs interact with multiple MTs (King and

Nicklas, 2000). However, since both yeast and vertebrate cells contain multiple chromosomes, two or more pairs of sister KTs could interact with the lateral surface of a single MT during prometaphase, and it is unknown how multiple KTs behave in this situation. For example, can they be transported by lateral sliding on a single MT, and can two (or more) of them establish end-on attachment to one MT? If only one KT is able to establish end-on attachment to one MT, what happens to other KTs on the same MT? Does it cause any problems and, if so, are there any mechanisms to mitigate such problems? In this study, we address these questions using the budding yeast *Saccharomyces cerevisiae* as a model organism.

Results

A single MT can accommodate only a single KT for sustained end-on attachment, leading to detachment of another KT on the MT lateral surface

To analyze individual KT–MT interactions in detail, we previously developed an engineered assay system, in which KT assembly was delayed on a chosen centromere by transcription from an adjacently inserted promoter (Tanaka et al., 2005). This increased the distance between the centromere and the mitotic spindle, allowing detailed observation of KT–MT interactions, after inducing KT assembly on the centromere by turning off the transcription (centromere re-activation assay; Figure S1A). To address whether two KTs can interact with a single MT, we modified this assay to regulate KT assembly on two centromeres (two pairs of sister centromeres) on different chromosomes (chromosome *III* and *XV*). After KT assembly was induced on both centromeres, they were able to interact with the lateral surface of the same or different MTs extending from a spindle pole. We focused on the former case, where both centromeres are caught on the same single MT (Figure 1B, step 1). A single MT was discerned as reported previously, i.e. by comparing its fluorescent signal with a cytoplasmic MT that is known to be single (Figure S4 in Tanaka et al., 2005). In these cases, the two centromeres moved by sliding along the MT lateral surface towards a spindle pole (Figure 1B, step 1; Figure 1C). Thus, a single MT can accommodate lateral attachment and allow sliding of two KTs.

In some cases, the centromere more distal to the spindle pole was subsequently tethered by end-on attachment to the plus end of a shrinking MT, and continued moving towards the spindle pole by end-on pulling as the MT shrunk (Figure 1B, step 2; Figure 1D, 143 s). Such end-on attached centromeres often caught up (came into contact) with

the laterally attached more proximal centromere on the same MT (Figure 1B, step 3; Figure 1D, 195 s, 'contact'). In this situation, both centromeres were co-transported poleward at the end of a shrinking MT, for a short distance, following such contact (Figure 1D, 208 s). Subsequently, the proximal centromere, that had originally been laterally attached prior to the contact, became detached from the MT end (or its proximity), while the original distal centromere continued moving towards the pole by end-on pulling of the shrinking MT (Figure 1D, 234 and 247 s). Another example of centromere detachment is shown in Figure S1B. We observed 94 events, in which an end-on attached centromere came into contact with a laterally attached centromere. 28 events out of such 94 events led to centromere detachment. Crucially, in all centromere detachment events, the laterally attached, rather than the end-on attached, centromere showed detachment following the contact. There was no particular bias in the detachment frequency between the two centromeres; the centromeres on chromosome *III* and *XV* showed 15 and 13 detachments, respectively. In addition, the speed of co-transport of two KTs (on the two marked centromeres) was faster than KT lateral sliding, but slower than KT end-on pulling, on average (Figure S1C).

It is noteworthy that KT detachment occurred at an approximately constant rate during co-transport after two KTs came into contact (Figure S1D). The majority of KT detachment (~80%) happened before KTs had moved more than 2 µm by co-transport. We assume that, after one KT establishes attachment to the end of a depolymerizing MT, another KT may still remain attached at the proximity of the MT end for a short period, and thus be co-transported, but would eventually detach from the MT end (Figure S1E, left). Alternatively, two relevant chromosomes may be entangled around two KTs for a short period, causing KT co-transport. In any case, if co-transported KTs reached a spindle pole, we were rarely able to detect KT detachment from a pole. We speculate that most KTs that are detached in the immediate vicinity of a spindle pole might be recaptured rapidly by MTs that are in a particularly high density near the pole (Kitamura et al., 2010; Winey et al., 1995), but this would be indiscernible in our assay. There are several short MTs (about 200 nm) extending from the spindle pole (Kitamura et al., 2010; Winey et al., 1995), which would also contribute to rapid recapture of KTs detached in the vicinity of a pole. Alternatively, chromosome crowding in the vicinity of a spindle pole may prevent KTs from dispersing, following their detachment from MTs. In conclusion, we find that a single MT can accommodate only one KT (one pair of sister KTs) for sustained end-on attachment, leading to detachment of other, laterally attached, KTs from the MT plus ends.

When sister chromatid cohesion is lost, sister KTs exclude each other from sustained end-on MT attachment

The above results suggest that there is a limited capacity of the KT to form an end-on attachment. One KT (one pair of sister KTs) seems to form an 'exclusive' attachment to the MT end. What comprises such an exclusive attachment? Are both sister KTs involved or is one sister KT sufficient to make it? Sister KTs are normally connected by sister chromatid cohesion at the centromere region (Tanaka et al., 2013). If this cohesion is lost, sister KTs separate from each other, but each sister can still interact with a MT (Tanaka et al., 2000). In this situation, do sister KTs exclude each other from formation of end-on attachment on a single MT, as do two pairs of sister KTs? To address this question, we depleted the cohesin subunit Scc1 (also called Mcd1), and investigated how such separated sister KTs interact with MTs. We used the centromere reactivation assay to analyze individual KT–MT interaction in detail in this condition (Figure S1A). We focused on situations where two sister KTs were initially caught on the lateral surface of the same MT (Figure 2A). Subsequently one sister KT, usually the one distal to the spindle pole, was often 'tethered' at the MT end and moved towards a spindle pole as the MT shrinks, indicating end-on attachment (Figure 2B, 50 s). This end-on attached KT then caught up with its sister on the MT lateral surface (60 s, 'contact'), which led to detachment of one sister KT from the MT end (80 s). In total, we observed 17 examples of sister KT detachment (following 52 contact events). As the two sister KTs could not be distinguished in this situation, we were not certain which sister KT showed detachment. Nonetheless, we assumed that it was the KT originally on the MT lateral surface that showed detachment, based on our analogous observation of two pairs of sister KTs (Figure 1B, D). In conclusion, if cohesion is lost, two separate sister KTs exclude each other from the end-on MT attachment.

The results so far suggest that there is a limited capacity of the KT to form sustained end-on attachment. In fact, once one KT (pair of sister KTs) forms an end-on attachment, another KT cannot form a sustained end-on attachment on the same MT, and any KT on the MT lateral surface shows detachment after it comes into contact with the end-on attached KT (Figure 1B, D). The same thing happens if two sister KTs separate from each other due to a loss of cohesion i.e. once one sister KT forms an end-on attachment, it excludes the other sister making sustained end-on attachment (Figure 2A, B). Thus, a single sister KT is sufficient to establish 'exclusive' end-on attachment (Figure S1E, right). One possible interpretation of the limited KT capacity for the attachment to the MT end is that, once a single KT attaches at the MT end, it takes

up MT binding sites with a strong affinity and thus sterically excludes other KTs from achieving a high affinity stable attachment.

KT lateral sliding along a MT delays and diminishes discernible KT detachment caused by a contact with another KT at the MT end

As shown above, a KT on the MT lateral side shows detachment if it comes into contact with another KT that is attached to the end of the same MT. If such detachment happens frequently, it could compromise efficient KT collection to the spindle, or to a spindle pole in yeast. Is there any mechanism to mitigate such adverse effects? We envisaged that KT lateral sliding along the MT might contribute to such mitigation by moving laterally attached KTs towards a spindle pole before end-on attached KTs come into contact with, and detach, them. In budding yeast, lateral sliding of a KT is driven by the minus-end directed kinesin, Kar3 (kinesin-14), which localizes at the KT (Tanaka et al., 2007; Tanaka et al., 2005). To address the effects of a lack of KT sliding, we depleted Kar3 and compared the number of KT detachments with those in Kar3 wild-type cells. We used the centromere reactivation assay (Figure S1A) with two reactivated centromeres. To obtain the number of samples required for optimal statistical analysis, we conducted the experiments in an Slk19-depletion background, which diminished the association between the two marked *CEN*s (two pairs of sister *CEN*s) in this experimental setting (Richmond et al., 2013). Slk19 depletion did not affect the KT sliding function of Kar3 (Figure S2A).

As expected, KT sliding was abolished after Kar3 depletion (Figure S2A). In both Kar3-depleted and Kar3 wild-type cells, a laterally attached KT showed detachment after coming into contact with an end-on attached KT; Figure 3A shows an example of a Kar3-depleted cell. The rate of KT detachment after the contact was similar in the two cells (Figure S2B). We then analyzed the position (distance from a spindle pole) of 1) the initial KT capture by a MT, 2) an end-on attached KT coming into contact with a laterally attached KT, and 3) subsequent detachment of a laterally attached KT from the MT end (Figure 3B). A KT was caught on the lateral side of a MT at similar distances from a spindle pole in both Kar3 wild-type and Kar3-depleted cells (Figure 3C, left). However, in Kar3-depleted cells, end-on attached KTs came into contact with laterally attached KTs further away from a pole (Figure 3C, middle). In these cells, the KT detachment was detected more frequently, and at a greater distance from the spindle pole, than in Kar3 wild-type cells (Figures 3C right, and D). Why are the KT detachments following a contact more frequent in Kar3-depleted cells? As we

discussed in the first section, we reason that many KTs, detached in the immediate vicinity of a spindle pole might be indiscernible since they are often recaptured rapidly by MTs whose density is high in that region (Kitamura et al., 2010; Winey et al., 1995). In Kar3-depleted cells, more KT detachments following contacts occur at a greater distance from a spindle pole, which would make discernible detachments more frequent. We conclude that KT lateral sliding along a MT towards a spindle pole delays and diminishes discernible KT detachment after an end-on attached KT comes into contact with a laterally attached KT.

KT lateral sliding along a MT also delays and diminishes discernible KT detachment caused by a contact with another KT, in physiological conditions

So far we have used the centromere reactivation assay to study how two KTs interact with the same single MT (Figure S1A). We next addressed this in physiological conditions, without using the centromere reactivation assay, and without using Slk19 depletion. In physiological conditions, KTs are attached to MTs during most of the cell cycle in budding yeast (Winey and O'Toole, 2001). However, upon centromere DNA replication KTs at least partially disassemble, leading to detachment of centromeres from MTs (Kitamura et al., 2007). Kinetochores are reassembled and interact with MTs again within 1–2 minutes, making initially lateral, and then end-on attachment.

We visualized one centromere and KTs, and analyzed the cases where the marked centromere and one KT (on another centromere) interacted with presumably the same MT (see Materials and methods). We focused on the cases where the centromere was proximal, and the KT distal, to a spindle pole on the same MT (see Figure 4A, 140–180 s). We chose such cases for our analyses because of the reasons explained in Figure S3A. Figures S3B and 4A show examples of a Kar3 wild-type and Kar3-depleted cell, respectively. We confirmed that in Kar3-depleted cells the centromere did not show sliding to a spindle pole, as expected (Figure S3C). After the KT on the MT end came into contact with the centromere (Figure 4A, 190 s), the centromere detached from the MT end (220 s), similarly to what we observed in the centromere reactivation assay. The rate of centromere detachment after the contact events was similar in Kar3 wild-type and Kar3-depleted cells (Figure S3D). We then compared the position (distance from a spindle pole) of the centromere upon the following key events (Figure 4B): In Kar3 wild-type and Kar3-depleted cells, the centromere was caught at similar distances from a spindle pole (Figure 4C, left). However, in Kar3-depleted cells, laterally attached centromere came into contact with end-on attached KTs further away from a pole, than

in Kar3 wild-type cells (Figure 4C, middle). Then, in Kar3-depleted cells, the centromere detachment following the contact happened more frequently and further from a pole (Figures 4C right, and D). As discussed in the previous section, we speculate that detachment of centromeres in the vicinity of a spindle pole might often be indiscernible because they are quickly recaptured by MTs whose density is high around a spindle pole. We conclude that, in physiological conditions, KT lateral sliding along a MT delays and diminishes discernible KT detachment caused by a contact with an end-on attached KT.

Lateral KT sliding shortens the time required for collecting the complete set of KTs to a spindle pole, by delaying KT detachments

The detachment of laterally attached KTs, after coming into contact with end-on attached KTs, may delay collection of all KTs to a spindle pole, which could then compromise the fidelity of subsequent bi-orientation establishment (see Discussion). We next aimed to evaluate how the KT detachment affects overall KT collection to a spindle pole, but it was difficult to address this using live-cell imaging because we could not visualize all the KTs; the intensity of some KTs was too weak to observe (Kitamura et al., 2007). We therefore employed a mathematical simulation (see Materials and methods). We simulated the following process (Figure 5A): A yeast cell carries 16 chromosomes, and all 16 centromeres are tethered to short MTs (100–200 nm) in the vicinity of a spindle pole in G1 phase (Kitamura et al., 2010; O'Toole et al., 1999). Upon DNA replication, KTs disassemble and centromeres move away from a spindle pole (Kitamura et al., 2007). Within 1–2 minutes KTs reassemble, allowing centromeres to again interact with MTs, making lateral attachment initially and then end-on attachment. Subsequently, KTs slide along MTs and move further by end-on pulling towards a spindle pole. If an end-on KT comes into contact with a laterally attached KT on the same MT, the lateral one shows detachment after KT co-transport for a short period (Figure 5B), as we found in live cells, above. For the simulation, the average speed of KT displacement along a MT was estimated by live-cell imaging in Figure S4A, and other parameter values for MT dynamics and KT motions were obtained from previous studies (Gandhi et al., 2011; Kalinina et al., 2013; Kitamura et al., 2007; Kitamura et al., 2010; Tanaka et al., 2007).

Using this simulation, we 'switched off' the KT sliding and compared the outcome with that from the 'wild-type' condition in which KT sliding was normal. In the absence of sliding, we found that 'discernible' KT detachment happened more frequently and at a

greater distance from a spindle pole, after coming into contact with an end-on attached KT (Figure 5C; sliding plus and minus, compare blue and red). These results are consistent with the results of live-cell imaging in physiological conditions (see Figure 4C, D). Note that, in the simulation, we defined 'discernible' KT detachment as a minimum of 30 s before subsequent recapture by a MT, since we could not detect recapture in less than 30 s by live-cell imaging. The simulation also largely recapitulates both the position and frequency of KT detachments in live-cell imaging (Figure S4B, C). Next we compared the total KT collection time i.e. time from first centromere detachment from a spindle pole until the last centromere reaching a pole and forming end-on attachment. In the absence of sliding, the distribution of total KT collection time was shifted towards the right (Figure 5D; sliding plus and minus, compare blue and red). Thus, in the simulation, KT sliding enhances efficiency of KT collection to a spindle pole and shortens total KT collection time.

KT sliding along a MT could shorten the total KT collection time either by bringing KTs more rapidly towards a spindle pole or by diminishing KT detachment (as a result of delaying contact between end-on and laterally attached KTs). Which effect contributes most to shortening the total KT collection time? To address this question, we analyzed total KT collection time by the simulation after making KT detachment frequency without KT sliding similar to that with KT sliding. The KT detachment frequency became similar with and without KT sliding, when the parameter value defining the KT detachment rate was reduced to 9.4 % without KT sliding (Figure 5C, compare green and blue). Intriguingly, when KT sliding was absent, the reduced detachment led to a shift of total KT collection time to the left (Figure 5D, shift from red to green). This suggests that lateral KT sliding reduces total KT collection time by, at least partly, diminishing KT detachment. When compared, diminishing KT detachment seems to contribute more to shortening total KT collection time (shift from red to green in Figure 5D) than does bringing KTs more rapidly to a spindle pole (shift from green to blue in Figure 5D). After frequent KT detachment in the absence of KT sliding, some detached centromeres require a long time for recapture, which leads to a prolonged total KT collection time (Figures S4D–G). In conclusion, the simulation suggests that the KT lateral sliding along MTs diminishes the KT detachment, caused by contact with end-on attached KTs, and thus contributes to shortening total KT collection time.

Discussion

Proper chromosome segregation in mitosis relies on chromosome bi-orientation, i.e. attachment of sister KTs to the ends of MTs extending from the opposite spindle poles (Kalantzaki et al, 2015). How could KTs establish bi-orientation efficiently? A KT (pair of sister KTs) initially interacts with the MT lateral surface, which provides a much larger contact surface than does the MT end. This ensures an efficient encounter between the KT and a MT (Rieder and Alexander, 1990; Tanaka et al., 2005). The KT then needs 1) to establish attachment to the MT end (end-on attachment) and 2) to be transported to the vicinity of a spindle pole (KT collection) in budding yeast, where the bipolar spindle is subsequently formed; or to the centre of the spindle in metazoan cells, where many MTs extend from both spindle poles at high density (Kitamura et al., 2007; Shrestha and Draviam, 2013; Tanaka et al., 2007). To do so, in principle the KT could establish end-on attachment first and then could be transported towards the spindle as the MT shrinks (end-on pulling). Indeed this strategy could work well in a cell with only a small number of chromosomes. However, our results suggest that if cells have many chromosomes they need the second mechanism of KT transport for efficient KT collection. In fact, the MT end can accommodate only one KT (pair of sister KTs) for sustained end-on pulling, and if multiple KTs are on the same MT they detach from the MT end except for the first KT to form an end-on attachment (Figure 1B, D). Frequent detachments prolong the time required for collection of the complete set of KTs (Figure 5D). To reduce the frequency of detachments, a KT can be transported, by sliding, along a MT towards the spindle (or spindle pole) before the end of a shrinking MT (on which another KT could be attached) reaches it, i.e. the lateral sliding can delay and diminish discernible KT detachment. This explains why vertebrate cells and budding yeast are equipped with a mechanism for promoting KT sliding along a MT; i.e. in these cells, MT minus end-directed motors, dynein and Kar3 (kinesin-14), localize at KTs and drive KT sliding (Tanaka et al., 2007; Vorozhko et al., 2008; Yang et al., 2007).

Human cells and the budding yeast *S. cerevisiae* (diploid in natural environment) carry 46 and 32 chromosomes, respectively. However, in cells with much fewer chromosomes, KT detachments would be rare even without KT sliding. Therefore, if the major role of KT sliding were indeed to diminish KT detachments, we would postulate that KTs might not undergo sliding along a MT in cells with fewer chromosomes. Fission yeast *Schizosaccharomyces pombe* (haploid in natural environment) carries only three chromosomes, and this organism notably lacks a mechanism of KT sliding along a MT (Franco et al., 2007; Grishchuk and McIntosh, 2006). In *S. pombe*, kinesin-14 Klp2 still

localizes at KTs (Gachet et al., 2008; Grishchuk and McIntosh, 2006), but may have lost the ability to drive KT sliding along a MT while the number of chromosomes was reduced during the evolution of *S. pombe* (Dujon, 2010). It will be intriguing to address if KT sliding along a MT is present or absent in more organisms carrying a variety of numbers of chromosomes.

Meanwhile, in vertebrate cells, it is still unclear how frequently two or more kinetochores could attach to one MT in early mitosis and how frequently an end-on attached KT comes into contact with a laterally-attached KT. In any case, vertebrate KTs are larger than budding yeast KTs and may show a greater steric exclusion once establishing end-on attachment. For example, an end-on attached KT may more readily exclude a laterally attached KT when they come into contact in vertebrate cells, leading to more quick detachment (i.e. after a shorter period of co-transport) of the laterally attached KT, than in budding yeast. Nonetheless, dynein can drive KT sliding at a higher speed in vertebrate cells than Kar3 (Tanaka et al., 2007; Vorozhko et al., 2008; Yang et al., 2007); thus discernible KT detachment might be more effectively diminished in vertebrate cells. It is an important research topic how vertebrate cells mitigate problems with multiple KTs on one MT in early mitosis.

Materials and methods

Yeast strains and cell culture

The background of yeast strains (W303) and the methods for yeast culture have been described previously (Amberg et al., 2005; Tanaka et al., 2007). The genotypes of strains used in this study are shown in Table S1. To synchronize cells in the cell cycle, yeast cells were arrested in G1 phase by treatment with yeast mating pheromone (α- or a-factor) and subsequently released to fresh media (Amberg et al., 2005; O'Reilly et al., 2012). The a-factor was synthesized as reported previously (O'Reilly et al., 2012). Cells were cultured at 25ºC in YPA medium containing 2% glucose (YPAD) unless otherwise stated. To activate the *GAL* promoter, cells were pre-incubated in medium containing 2% raffinose (without glucose) for at least for 3 hours, and subsequently incubated in medium containing both 2% galactose and 2% raffinose. Cells were incubated in medium containing 2% glucose to suppress the *GAL* promoter (without subsequent activation). The *MET3* promoter was activated by incubation of cells in methionine drop-out media, and suppressed by adding 2 mM methionine to the relevant media. Constructs of *CEN15-tetOs*, *CEN5-tetOs* (Tanaka et al., 2000), P_{GAL}-*CEN3-tetOs* (Hill

and Bloom, 1987; Michaelis et al., 1997; Tanaka et al., 2005), *TetR-3×CFP* (Bressan et al., 2004; Michaelis et al., 1997), *P_{MET3}-CDC20* (Uhlmann et al., 2000), *GFP-TUB1* (Straight et al., 1997), were described previously. *P_{GAL}-CEN3-lacOs* was constructed similarly to *P_{GAL}-CEN3-tetOs* (replacing *CEN3* on chromosome *III*) but designed to replace *CEN15* on chromosome *XV*; this was visualized with GFP-LacI that bound *lacO*s (Straight et al., 1996). The *pDH20* plasmid containing *YFP-TUB1* was obtained from Yeast Resource Centre (Seattle). The *NDC80* and *MTW1* genes were tagged with 4×*mCherry* at their C-terminus at their original gene loci by a one-step PCR using 4×*mCherry* cassette (pT909) as a PCR template (Maure et al., 2011).

Centromere reactivation assay

To analyze individual KT–MT interactions in detail, the centromere re-activation assay was used (Tanaka et al., 2010; Tanaka et al., 2005). In this assay, KT assembly was delayed on a chosen centromere (*CEN3-tetOs* or *-lacOs*, replacing *CEN3* on chromosome *III* and/or *CEN15* on chromosome *XV*) by transcription from *GAL* promoter. This increased the distance between the centromere and the mitotic spindle, allowing detailed observation of KT–MT interactions after inducing KT assembly on the centromere by turning off the *GAL* promoter in metaphase arrested cells (Figure S1A). Cells with *P_{GAL}-CEN3-tetOs* (or *-lacOs*) *P_{MET3}-CDC20* (see full genotypes in Table S1) were cultured as explained in the legend of Figure 1C.

Analysis of KT-MT interaction in physiological conditions

In our study of the initial KT–MT interaction in physiological conditions (Figure 4), we visualized one centromere and KTs because of the technical reasons explained in Figure S3A. We analyzed the cases where the centromere and one KT (on another centromere) on the same line of a MT signal (whose intensity is uniform along the line) extending from a spindle pole. In these cases, we reasoned that the visualized centromere and the KT of our interest are on the same MT, at least in the majority of the cases (even if not all cases). Supporting this notion, end-on pulling showed a higher velocity than did lateral sliding (Figure S3C), as found in the centromere reactivation assay (Figure S1C) where a single MT is more easily discernible; we would not expect this result if we often failed to discern single MTs and thus often mixed up end-on pulling with the lateral sliding.

Depletion of Scc1, Kar3 and Slk19

To deplete Scc1 protein, an anchor away system was used (Haruki et al., 2008), which consists of *SCC1-FRB* (C-terminal tag at the original *SCC1* locus)*, RPL13A-2×FKBP12,*

TOR1-1 and *fpr1*Δ. In the presence of rapamycin (10 µM), Scc1 protein bound Rpl13A ribosomal protein due to the FRB–FKBP12 interaction, which led to depletion of Scc1 in the nucleus. To deplete Kar3 and Slk19, *KAR3 and SLK19* were tagged with *aid* and *mini-aid* tags (auxin-inducible degron tags), respectively, at their C-termini at original loci in the strain carrying the rice F-box gene *TIR1* (Kubota et al., 2013; Nishimura et al., 2009). In the presence of auxin NAA (1 mM), *aid*-tagged proteins bound Tir1, leading to their ubiquitylation and degradation.

Live-cell imaging and image analyses

The procedures for time-lapse fluorescence microscopy were described previously (Tanaka et al., 2010). Time-lapse images were collected at 25ºC. Images were acquired using a DeltaVision Core or Elite microscope (Applied Precision), an UPlanSApo 100✕ objective lens (Olympus; NA 1.40), SoftWoRx software (Applied Precision), and a CoolSnap HQ (Photometrics). We acquired 7–9 (0.7 µm apart) z-sections, which were subsequently processed through deconvolution, and analyzed with Volocity (Improvision) software. CFP, GFP, and mCherry signals were discriminated using the 89006 multi-band filter set (Chroma). For the image panels in Figures, Z-sections were projected to two-dimensional images. Statistical analyses were carried out using Prism (Graph Pad) software.

Computer simulation of KT–MT interaction

We created a computer model and carried out simulations of the initial KT–MT interaction, based on configuration in physiological conditions (Figure 4; Kitamura et al., 2007). The simulation was previously developed (Gandhi et al., 2011; Vasileva et al., 2017), but several modifications were introduced in this study. The values of the majority of parameters were determined, based on previous studies (Gandhi et al., 2011; Kalinina et al., 2013; Kitamura et al., 2007; Kitamura et al., 2010; Tanaka et al., 2007; Tanaka et al., 2005), and some unknown parameter values were determined in the current study (Table S2).

The model was computed as a series of events on a constant time step Δt. All objects (MTs, KTs and Stu2) were located in a 3-dimensional space. The nucleus was represented by a sphere of radius R_{nuc}. An exclusion radius, r_{ex}, was established around the spindle pole. Each MT was a line segment extending into the nucleus from the spindle pole. Each KT was a point inside the nucleus. MTs could grow and shrink with speed v_{gro} and v_{shr}, respectively. Parameters defining their dynamics, such as the initial

MT number n_{MT}, MT catastrophe rate K_{cat}, MT beaming factor β, were set as in (Gandhi et al., 2011). When a growing MT hit the nuclear envelope, it started to shrink. When an empty MT shrank to r_{ex}, it could start growing at a certain nucleation rate K_{nuc}, unless there were KTs waiting at r_{ex}, in which case the MT captured the KT and showed no further change. The MTs also experienced 'pivoting', which was modeled by angular random walk with the diffusion coefficient D_{MT} (Brun, 2011; Kalinina et al., 2013). Stu2 was a MT polymerase that causes MT rescue (Gandhi et al., 2011) and its properties (Stu2 sending rate K_{stu2}, Stu2 speed v_{stu2}, probability of MT rescue P_{res}, KT rescue delay t_d) were defined as in (Gandhi et al., 2011). Time 0 was defined as the mean time of replication of the first *CEN* (*CEN2*) (Vasileva et al., 2017). When replicated, a centromere detached from a pole and could move freely by a random walk with diffusion coefficient D. After a delay t_{del}, a KT was reassembled at the centromere's position.

KTs also moved inside the nucleus (but not within the exclusion radius) with a diffusion coefficient D. Once attached to a MT, a KT moved laterally along a MT towards the spindle pole or was pulled by the distal end of the MT with speed v_{lat} or v_{pul}, respectively. Sliding motion was varied by a linear diffusion with a coefficient D_{lat}. When a sliding KT reached the exclusion radius r_{ex}, it remained there until an empty MT shrank to r_{ex}. Then, the KT was caught at the end of this MT; no further change occurred to such KT and MT, apart from MT pivoting. The same happened immediately when an end-on pulled KT reached r_{ex}.

The interaction between KT-generated and spindle-pole MTs was simplified by assuming a certain capture radius, R_{KT}, around each KT. If a KT was found at a distance R_{KT} from any part of a spindle-pole MT, the KT-derived MT connected to this spindle-pole MT by the shortest distance and brought the KT towards the spindle-pole MT, usually on its lateral side, at a speed v_{cap}. Once capture was completed, the KT began sliding, which was converted to end-on pulling if end-on attachment was subsequently established. The simulation was completed once all 16 reassembled KTs reached r_{ex} and established end-on attachment.

If an end-on pulled KT came into contact with another KT that was sliding along the same MT, they went into 'co-transport' mode. Both KTs travelled together at speed of v_{tran} while the sliding KT could detach (detachment) at a rate K_{evi}. In rare events where an end-on pulled KT came into contact with two (or more) other KTs on the lateral side of the same MT, K_{evi} was applied separately for the two others. We assumed that the

detached KT was not able to re-attach to a MT until the KT generated a MT from it at its maximum length R_{KT}; i.e. for R_{KT}/v_{gro} min (KT-derived MTs showed a similar growth rate to spindle-pole MTs; Kitamura et al., 2010).

The code for the simulation was written in Perl and simulations were run in a Linux environment. We ran 100,000 individual simulations in each condition. Detachments were counted and analyzed only if it took more than 0.5 min for detached KTs to be recaptured by a MT extending from a spindle pole; this is because KT detachment less than 0.5 min following detachment was difficult to recognize in live-cell imaging. To switch off KT sliding, the average KT displacement speed (which is normally 0.6 µm/min) was set at 0. To reduce the KT detachment frequency to 9.4%, KT detachment rate (which is normally 4.8/µm) was reduced to 0.45/µm.

References

Amberg, D. C., Burke, D. J. and Strathern, J. N. (2005). Methods in yeast genetics.

Bressan, D. A., Vazquez, J. and Haber, J. E. (2004). Mating type-dependent constraints on the mobility of the left arm of yeast chromosome III. *J Cell Biol* **164**, 361-71.

Brun, L. (2011). Search and capture model in different DNA segregation processes. In *Physics*, vol. PhD, pp. 64-88: EMBL, Heidelberg.

Cheerambathur, D. K. and Desai, A. (2014). Linked in: formation and regulation of microtubule attachments during chromosome segregation. *Curr Opin Cell Biol* **26**, 113-22.

Dujon, B. (2010). Yeast evolutionary genomics. *Nat Rev Genet.* **11**, 512-24.

Franco, A., Meadows, J. C. and Millar, J. B. (2007). The Dam1/DASH complex is required for the retrieval of unclustered kinetochores in fission yeast. *J Cell Sci* **120**, 3345-51.

Gachet, Y., Reyes, C., Courtheoux, T., Goldstone, S., Gay, G., Serrurier, C. and Tournier, S. (2008). Sister kinetochore recapture in fission yeast occurs by two distinct mechanisms, both requiring dam1 and klp2. *Mol Biol Cell* **19**, 1646-62.

Gandhi, S. R., Gierlinski, M., Mino, A., Tanaka, K., Kitamura, E., Clayton, L. and Tanaka, T. U. (2011). Kinetochore-dependent microtubule rescue ensures their efficient and sustained interaction in early mitosis. . *Dev Cell* **21**, 920-933.

Grishchuk, E. L. and McIntosh, J. R. (2006). Microtubule depolymerization can drive poleward chromosome motion in fission yeast. *EMBO J* **25**, 4888-96.

Haruki, H., Nishikawa, J. and Laemmli, U. K. (2008). The anchor-away technique: rapid, conditional establishment of yeast mutant phenotypes. *Mol Cell* **31**, 925-32.

Hill, A. and Bloom, K. (1987). Genetic manipulation of centromere function. *Mol Cell Biol* **7**, 2397-405.

Kalantzaki, M., Kitamura, E., Zhang, T., Mino, A., Novak, B. and Tanaka, T. U. (2015). Kinetochore-microtubule error correction is driven by differentially regulated interaction modes. *Nat Cell Biol.* **17**, 421-33.

Kalinina, I., Nandi, A., Delivani, P., Chacon, M. R., Klemm, A. H., Ramunno-Johnson, D., Krull, A., Lindner, B., Pavin, N. and Tolic-Norrelykke, I. M. (2013). Pivoting of microtubules around the spindle pole accelerates kinetochore capture. *Nat Cell Biol* **15**, 82-7.

King, J. M. and Nicklas, R. B. (2000). Tension on chromosomes increases the number of kinetochore microtubules but only within limits. *J Cell Sci* **113**, 3815-23.

Kitamura, E., Tanaka, K., Kitamura, Y. and Tanaka, T. U. (2007). Kinetochore microtubule interaction during S phase in Saccharomyces cerevisiae. *Genes Dev* **21**, 3319-30.

Kitamura, E., Tanaka, K., Komoto, S., Kitamura, Y., Antony, C. and Tanaka, T. U. (2010). Kinetochores generate microtubules with distal plus ends: their roles and limited lifetime in mitosis. *Dev Cell* **18**, 248-59.

Kubota, T., Nishimura, K., Kanemaki, M. T. and Donaldson, A. D. (2013). The Elg1 replication factor C-like complex functions in PCNA unloading during DNA replication. *Mol Cell* **50**, 273-80.

Maure, J. F., Komoto, S., Oku, Y., Mino, A., Pasqualato, S., Natsume, K., Clayton, L., Musacchio, A. and Tanaka, T. U. (2011). The Ndc80 loop region facilitates formation of kinetochore attachment to the dynamic microtubule plus end. *Curr Biol* **21**, 207-13.

Michaelis, C., Ciosk, R. and Nasmyth, K. (1997). Cohesins: chromosomal proteins that prevent premature separation of sister chromatids. *Cell* **91**, 35-45.

Nishimura, K., Fukagawa, T., Takisawa, H., Kakimoto, T. and Kanemaki, M. (2009). An auxin-based degron system for the rapid depletion of proteins in nonplant cells. *Nat Methods* **6**, 917-22.

O'Reilly, N., Charbin, A., Lopez-Serra, L. and Uhlmann, F. (2012). Facile synthesis of budding yeast a-factor and its use to synchronize cells of alpha mating type. *Yeast* **29**, 233-40.

O'Toole, E. T., Winey, M. and McIntosh, J. R. (1999). High-voltage electron tomography of spindle pole bodies and early mitotic spindles in the yeast Saccharomyces cerevisiae. *Mol Biol Cell* **10**, 2017-31.

Richmond, D., Rizkallah, R., Liang, F., Hurt, M. M. and Wang, Y. (2013). Slk19 clusters kinetochores and facilitates chromosome bipolar attachment. *Mol Biol Cell.* **24**, 566-77.

Rieder, C. L. and Alexander, S. P. (1990). Kinetochores are transported poleward along a single astral microtubule during chromosome attachment to the spindle in newt lung cells. *J Cell Biol* **110**, 81-95.

Shrestha, R. L. and Draviam, V. M. (2013). Lateral to end-on conversion of chromosome-microtubule attachment requires kinesins CENP-E and MCAK. *Curr Biol.* **23**, 1514-26.

Straight, A. F., Belmont, A. S., Robinett, C. C. and Murray, A. W. (1996). GFP tagging of budding yeast chromosomes reveals that protein-protein interactions can mediate sister chromatid cohesion. *Curr Biol* **6**, 1599-608.

Straight, A. F., Marshall, W. F., Sedat, J. W. and Murray, A. W. (1997). Mitosis in living budding yeast: anaphase A but no metaphase plate. *Science* **277**, 574-8.

Tanaka, K., Kitamura, E., Kitamura, Y. and Tanaka, T. U. (2007). Molecular mechanisms of microtubule-dependent kinetochore transport toward spindle poles. *J Cell Biol* **178**, 269-81.

Tanaka, K., Kitamura, E. and Tanaka, T. U. (2010). Live-cell analysis of kinetochore-microtubule interaction in budding yeast. *Methods* **51**, 206-13.

Tanaka, K., Mukae, N., Dewar, H., van Breugel, M., James, E. K., Prescott, A. R., Antony, C. and Tanaka, T. U. (2005). Molecular mechanisms of kinetochore capture by spindle microtubules. *Nature* **434**, 987-94.

Tanaka, T., Fuchs, J., Loidl, J. and Nasmyth, K. (2000). Cohesin ensures bipolar attachment of microtubules to sister centromeres and resists their precocious separation. *Nat Cell Biol* **2**, 492-9.

Tanaka, T. U. (2010). Kinetochore-microtubule interactions: steps towards bi-orientation. *EMBO J* **29**, 4070-82.

Tanaka, T. U., Clayton, L. and Natsume, T. (2013). Three wise centromere functions: see no error, hear no break, speak no delay. *EMBO Rep.* **14**, 1073-83.

Tanaka, T. U., Rachidi, N., Janke, C., Pereira, G., Galova, M., Schiebel, E., Stark, M. J. and Nasmyth, K. (2002). Evidence that the Ipl1-Sli15 (Aurora kinase-INCENP) complex promotes chromosome bi-orientation by altering kinetochore-spindle pole connections. *Cell* **108**, 317-29.

Uhlmann, F., Wernic, D., Poupart, M. A., Koonin, E. V. and Nasmyth, K. (2000). Cleavage of cohesin by the CD clan protease separin triggers anaphase in yeast. *Cell* **103**, 375-86.

Vasileva, V., Gierlinski, M., Yue, Z., O'Reilly, N., Kitamura, E. and Tanaka, T. U. (2017). Molecular mechanisms facilitating the initial kinetochore encounter with spindle microtubules. *J Cell Biol.* published online, doi: 10.1083/jcb.201608122.

Vorozhko, V. V., Emanuele, M. J., Kallio, M. J., Stukenberg, P. T. and Gorbsky, G. J. (2008). Multiple mechanisms of chromosome movement in vertebrate cells mediated through the Ndc80 complex and dynein/dynactin. *Chromosoma* **117**, 169-79.

Winey, M., Mamay, C. L., O'Toole, E. T., Mastronarde, D. N., Giddings, T. H., Jr., McDonald, K. L. and McIntosh, J. R. (1995). Three-dimensional ultrastructural analysis of the Saccharomyces cerevisiae mitotic spindle. *J Cell Biol* **129**, 1601-15.

Winey, M. and O'Toole, E. T. (2001). The spindle cycle in budding yeast. *Nat Cell Biol* **3**, E23-7.

Yang, Z., Tulu, U. S., Wadsworth, P. and Rieder, C. L. (2007). Kinetochore dynein is required for chromosome motion and congression independent of the spindle checkpoint. *Curr Biol* **17**, 973-80.

Figures

A — Lateral attachment → Lateral sliding → End-on attachment & pulling

Kinetochore   Spindle pole & microtubule

B
CEN
MT   CEN
Spindle

1. Both CENs lateral sliding → 2. End-on pulling Lateral sliding → Contact of two CENs → 3. Co-transport → 4. One CEN detached

C
CEN on Ch XV
0 s 340 360 380 400 420 460 560

Tubulin
CEN on Ch III

Merge
0 s

Spindle
CEN on Ch XV
CEN on Ch III

Plus end of suspected overlapping MT

Capture by MT

Distance from a spindle pole (μm)
Time (seconds)

MT length
CEN on Ch III   CEN on Ch XV

D
Contact Co-transport Detachment

CEN on Ch XV
13 s 91 143 195 208 234 247 286

Tubulin
CEN on Ch III

Merge

CEN on Ch XV
CEN on Ch III

Spindle   CEN on Ch XV   CEN on Ch III

Capture by MT
End-on
Contact
Detachment

Distance from a spindle pole (μm)
Time (seconds)

MT length
CEN on Ch III   CEN on Ch XV

Figure 1. A single MT accommodates two KTs with lateral attachment but only one KT with sustained end-on attachment

A) Diagrams explaining how a KT is captured and transported by a MT in eukaryotic cells. The KT initially interacts with the lateral surface of a single MT (lateral attachment), which extends from a spindle pole; the KT is then transported along the MT lateral surface towards a spindle pole by sliding (lateral sliding). Subsequently, the KT is tethered at the end of a single MT (end-on attachment) and transported polewards as the MT shrinks (end-on pulling) (Tanaka, 2010).

B) Diagrams summarizing the interaction between a single MT and two KTs (two pairs of sister KTs on the indicated *CEN*s). Two indicated *CEN*s were under control of the *GAL* promoter and visualized as fluorescent dots, and were inactivated, and subsequently reactivated, as in Figure S1A, to study their interaction with a MT in detail. After both *CEN*s were loaded on the lateral surface of a single MT, they showed sliding along the MT. In some cases, one *CEN* underwent conversion to end-on attachment, was transported by end-on pulling, and subsequently came into contact with the other *CEN*. Then, after brief co-transport, the *CEN* originally proximal to the spindle pole showed detachment. Note that either or both *CEN*s could reach a spindle pole from any of these stages without going through subsequent stages.

C) Representative example in which two KTs showed lateral sliding along a single MT. Cells (T6519) carry P_{GAL}-*CEN3-tetOs* (replacing *CEN15* on chromosome *XV*) *TetR-3×CFP* P_{GAL}-*CEN3-lacO* (replacing *CEN3* on chromosome *III*) *GFP-LacI YFP-TUB1* P_{MET3}-*CDC20*, where *tetO*s are tetracycline operators, TetR is the tetracycline repressor, *lacO*s are lactose operators, and LacI is the lactose repressor. GFP, YFP and CFP are green, yellow and cyan fluorescent protein, respectively. The GFP and YFP signals were collected together (green) while CFP signals were acquired separately (red). These cells were treated as in Figure S1A, i.e. were cultured overnight in methionine drop-out media with raffinose, treated with a mating hormone for 2.5 hours (to arrest in G1 phase), and released to fresh media with raffinose, galactose and 2 mM methionine (for Cdc20 depletion and P_{GAL}-*CEN* inactivation). After 4 hours, cells were suspended in synthetic complete medium containing glucose and methionine (to reactivate P_{GAL}-*CEN*). After 10 minutes incubation, images were acquired every 20 s for 30 min. Time zero is set arbitrarily. *Ch III*: chromosome III. *Ch XV*: chromosome XV. Left shows a representative cell while right shows its profile, i.e. graphs of length of the MT, which interacted with two *CEN*s, and positions of two *CEN*s (distance from a spindle pole; dashed red and green lines represent *CEN*s not on the MT, while solid red and green lines represent *CEN*s on the MT). See Supplemental Movie 1. T9717 cells (see D) showed similar results (Figure S1B).

D) Representative example where a laterally-attached KT showed detachment after coming into contact with an end-on attached KT. Cells (T9717) with the same genotype as T6519 (see C), except for carrying *GFP-TUB1* instead of *YFP-TUB1*, were treated as in C, and images (GFP and CFP signals) were acquired every 13 s. Graph on right shows the MT length and *CEN* positions as in C. See Supplemental Movie 2. Another example of KT detachment is shown in Figure S1B.
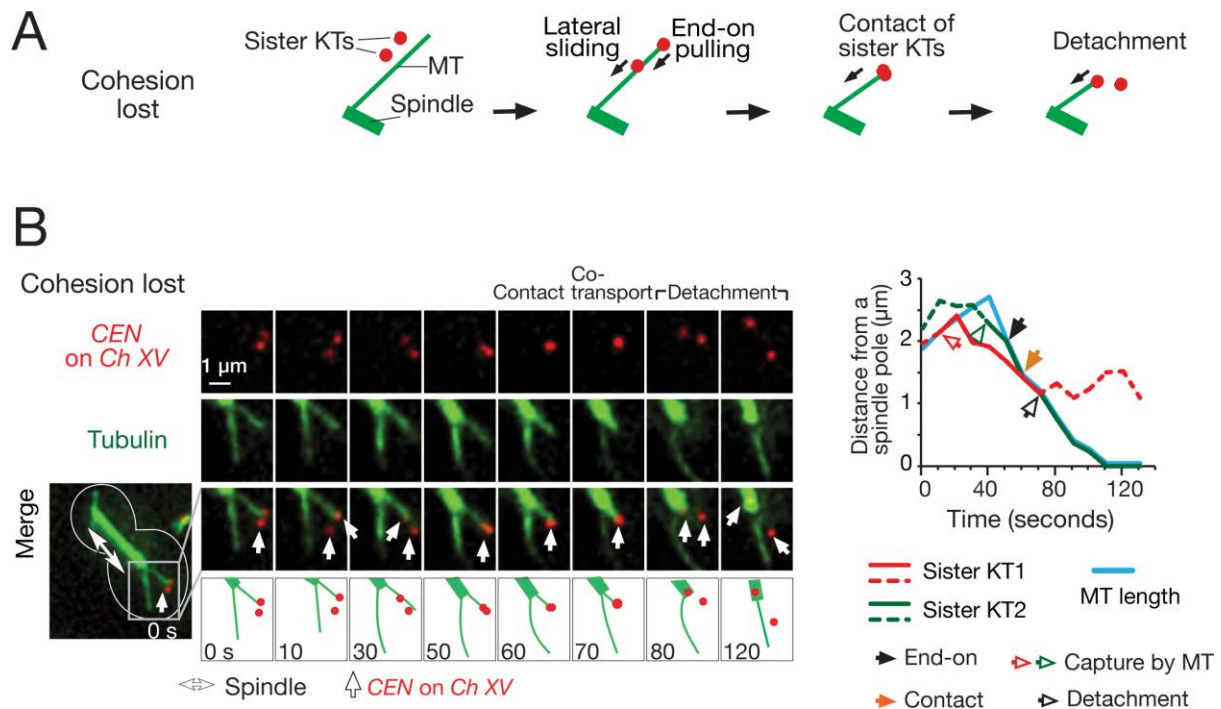
Figure 2. When sister chromatid cohesion is lost, sister KTs exclude each other from sustained end-on MT attachment

A) Diagrams summarizing the interaction of sister KTs with a single MT when cohesion is lost. When cohesion is lost and two sister KTs separate, a laterally attached sister KT detached from the MT end after coming into contact with an end-on attached sister KT.
B) Representative example where sister KTs interact with a single MT after their cohesion is lost. This interaction was followed by detachment of one sister KT. Cells (T11941) with *Scc1-AnchorAway P_{GAL}-CEN3-tetO TetR-3×CFP GFP-TUB1 P_{MET3}-CDC20* were treated as in Figure 1D, except that rapamycin was added upon release from G1 arrest (to deplete Scc1). Images (GFP and CFP signals) were acquired every 10 seconds. Graph (right) shows the MT length and the position of *CEN*s, as in Figure 1C. Note that the spindle elongates after Scc1 depletion, although cells are arrested in metaphase (Tanaka et al., 2000). See Supplemental Movie 3.
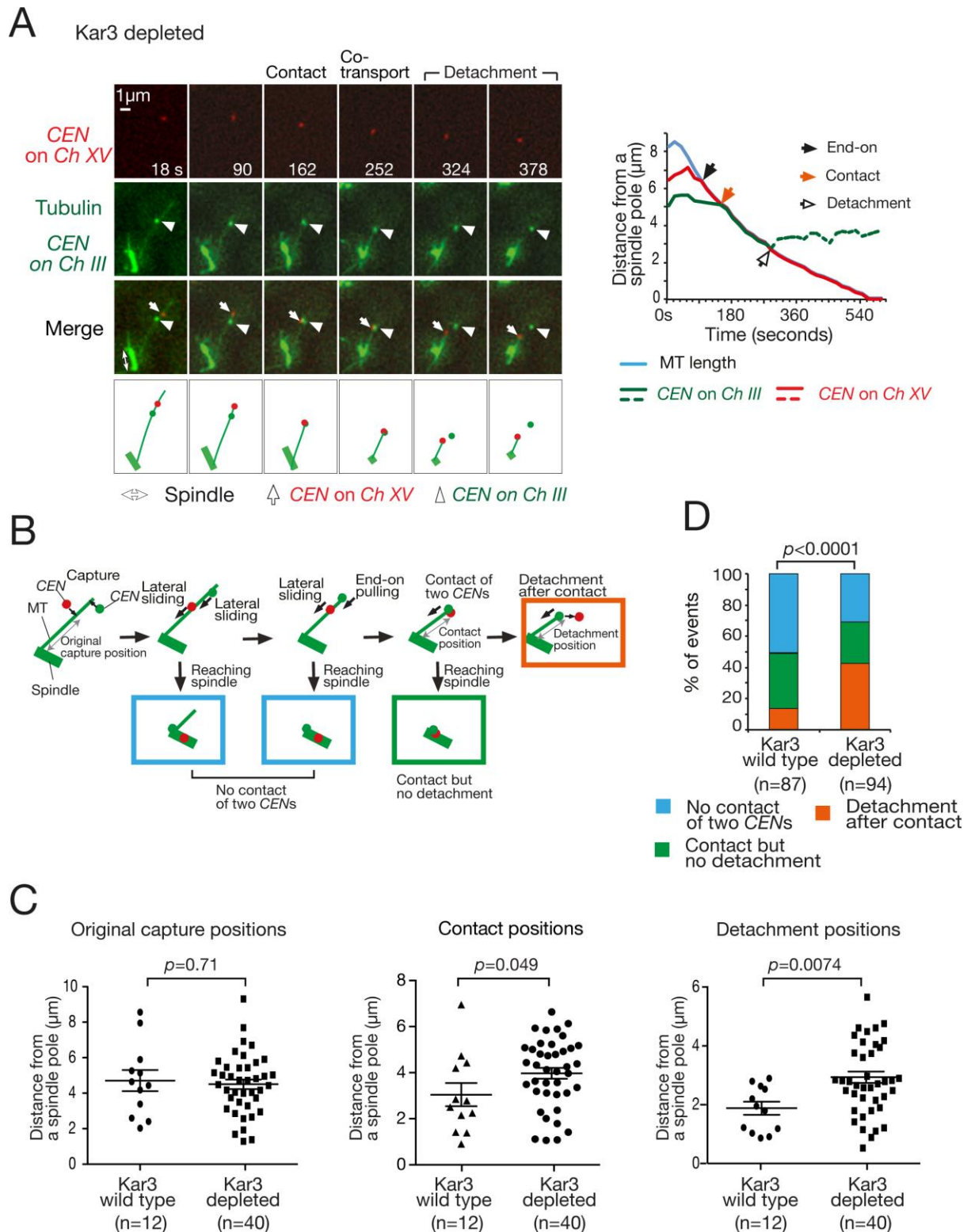
Figure 3. KT lateral sliding along a MT diminishes discernible KT detachment that occurs after coming into contact with an end-on attached KT.

A) Representative example of a Kar3-depleted cell where a laterally-attached KT showed detachment after coming into contact with an end-on attached KT. Cells (T11469) carrying *kar3-aid slk19-mini-aid TIR P*_{GAL}*-CEN3-tetOs* (replacing *CEN15* on

chromosome *XV*) *TetR-3×CFP P~GAL~-CEN3-lacO* (replacing *CEN3* on chromosome *III*) *GFP-LacI GFP-TUB1 P~MET3~-CDC20* were treated as in Figure 1C, except that 1-naphthaleneacetic acid (NAA) was added to deplete Kar3 and Slk19 when cells were released from G1 arrest. Images (GFP/YFP and CFP signals) were acquired every 18 s. Graph (right) shows the MT length and the position of *CEN*s, as in Figure 1C. See Supplemental Movie 4.

B) Diagrams explaining analyses in C and D. 'Original capture position', 'Contact position' and 'Detachment position' were measured as shown here and plotted in C. Rectangles in color represent the categorized situations shown in D in the same color.

C) In the absence of KT sliding, contact between two *CEN*s and subsequent detachment of *CEN* happen further from a spindle pole. Graphs show the initial capture positions (distance from a spindle pole) of *CEN*s (only those that subsequently showed detachment; left; see B), positions of end-on attached *CEN* coming into contact with laterally attached *CEN* (middle; see B) and the positions of *CEN* detachments (right; see B). T11469 cells (see A) and T11497 cells (*KAR3+ slk19-mini-aid*, otherwise the same as T11469 cells) were treated and images were acquired as in A. Graphs show individual data points and mean ± SEM. *p* values were obtained by *t*-test.

D) In the absence of KT sliding, *CEN* detachment is observed more frequently. Following the situation where two *CEN*s formed a lateral attachment on the same MT, one of the following three events took place (see B): 1) both *CEN*s reached a spindle pole without one coming into contact with the other (blue), 2) after one C*EN* formed end-on attachment, it came into contact with the other *CEN* and the two *CEN*s were co-transported to the spindle pole (green), or 3) after one C*EN* formed end-on attachment, it came into contact with the laterally attached *CEN*, which subsequently detached from the MT end (orange). Images acquired in A were used for this analysis. The graph shows the percentage of each event. The *p* value was obtained by a *chi*-square test for trend (the order for the trend was blue, green and orange).
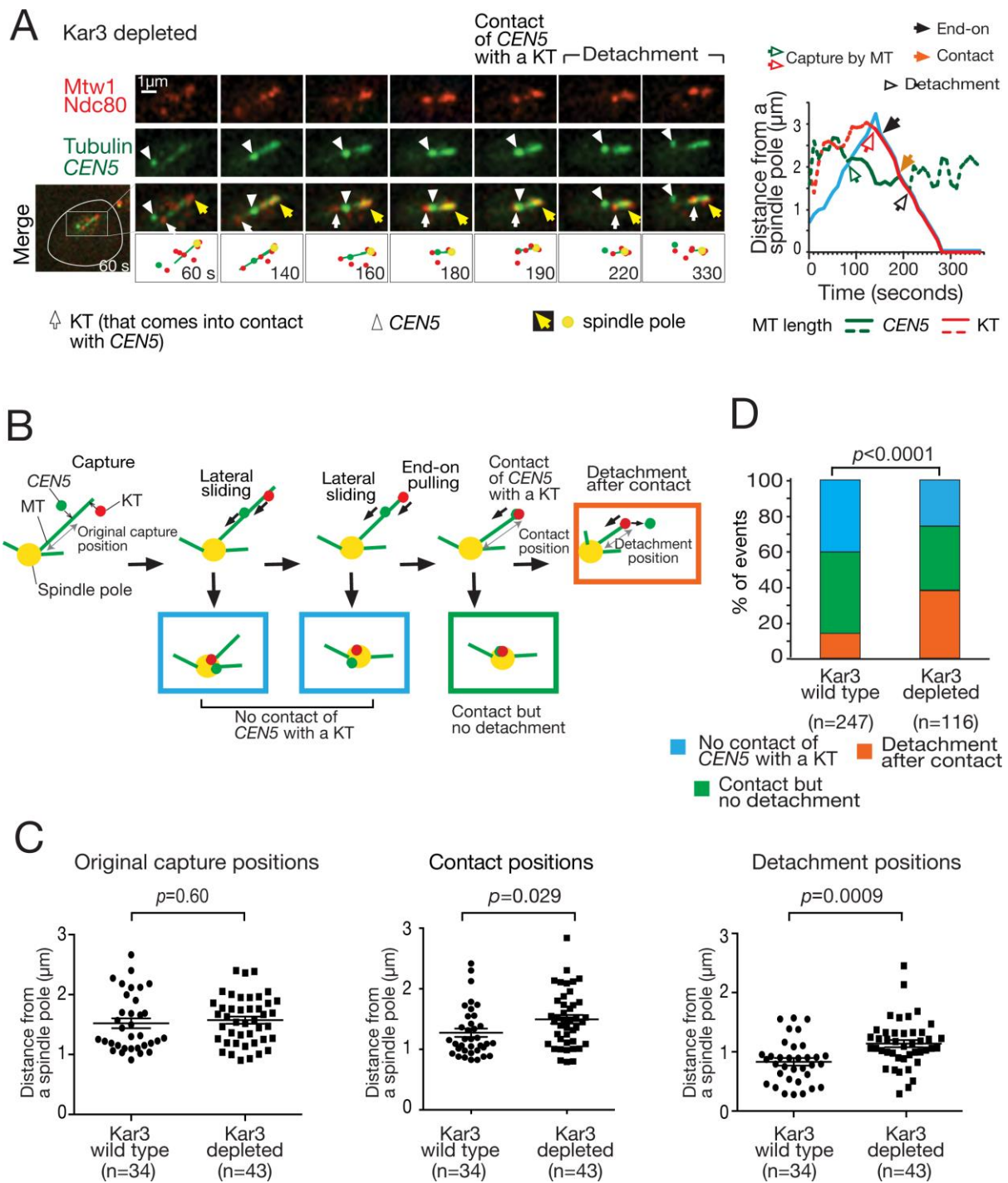
Figure 4. KT detachment is found in physiological conditions, after an end-on attached KT coming into contact with a laterally attached KT.

A) Representative example of centromere detachment in a Kar3-depleted cell with physiological condition. Cells (T11434) with *kar3-aid TIR1 CEN5-lacOs GFP-LacI GFP-TUB1 MTW-4×mCherry NDC80-4×mCherry* were treated with a mating pheromone for 3 hours (to arrest in G1 phase) and released into fresh medium. NAA was added for the last 30 min in G1 arrest and also after release from the arrest (to deplete Kar3). 30 min

after release from the G1 arrest, images (GFP and mCherry signals) were acquired every 10 s. See Supplemental Movie 5. A representative example of a Kar3 wild-type cell is shown in Figure S3B.

B) Diagrams explaining analyses in C and D. 'Original capture position', 'Contact position' and 'Detachment position' were measured as shown here and plotted in C. Rectangles in color represent the categorized situations shown in D in the same color.

C) In the absence of KT sliding, contact between a KT (not at *CEN5*) and *CEN5* and subsequent detachment of *CEN5* happen further from a spindle pole. Graphs show the initial capture position (distance from a spindle pole) of *CEN5* (only those that subsequently showed detachment; left; see B), the position of KT coming into contact with *CEN5* (middle; see B) and the positions of *CEN5* detachment (right; see B). T11434 cells (see A) and T11435 cells (*KAR3*+, otherwise the same as T11434 cells) were treated and images were acquired, as in A. Graphs show individual data points and mean ± SEM. The *p* values were obtained by *t*-test.

D) In the absence of KT sliding, *CEN5* detachment happens more frequently in physiological conditions. Images acquired in A were used for this analysis. Following the situation where a KT (not on *CEN5*) and *CEN5* formed a lateral attachment on presumably the same MT (the KT is more distal to a spindle pole than *CEN5*), one of the following three events took place (see B): 1) both the KT and *CEN5* reached a spindle pole without contact (blue), 2) after the KT formed end-on attachment, it came into contact with *CEN5* and they were co-transported to the spindle pole (green), or 3) after the KT formed end-on attachment, it came into contact with *CEN5* and *CEN5* showed detachment (orange). Images acquired in A were used for this analysis. The graph shows the percentage of each event. The *p* value was obtained by a *chi*-square test for trend as in Figure 3D.
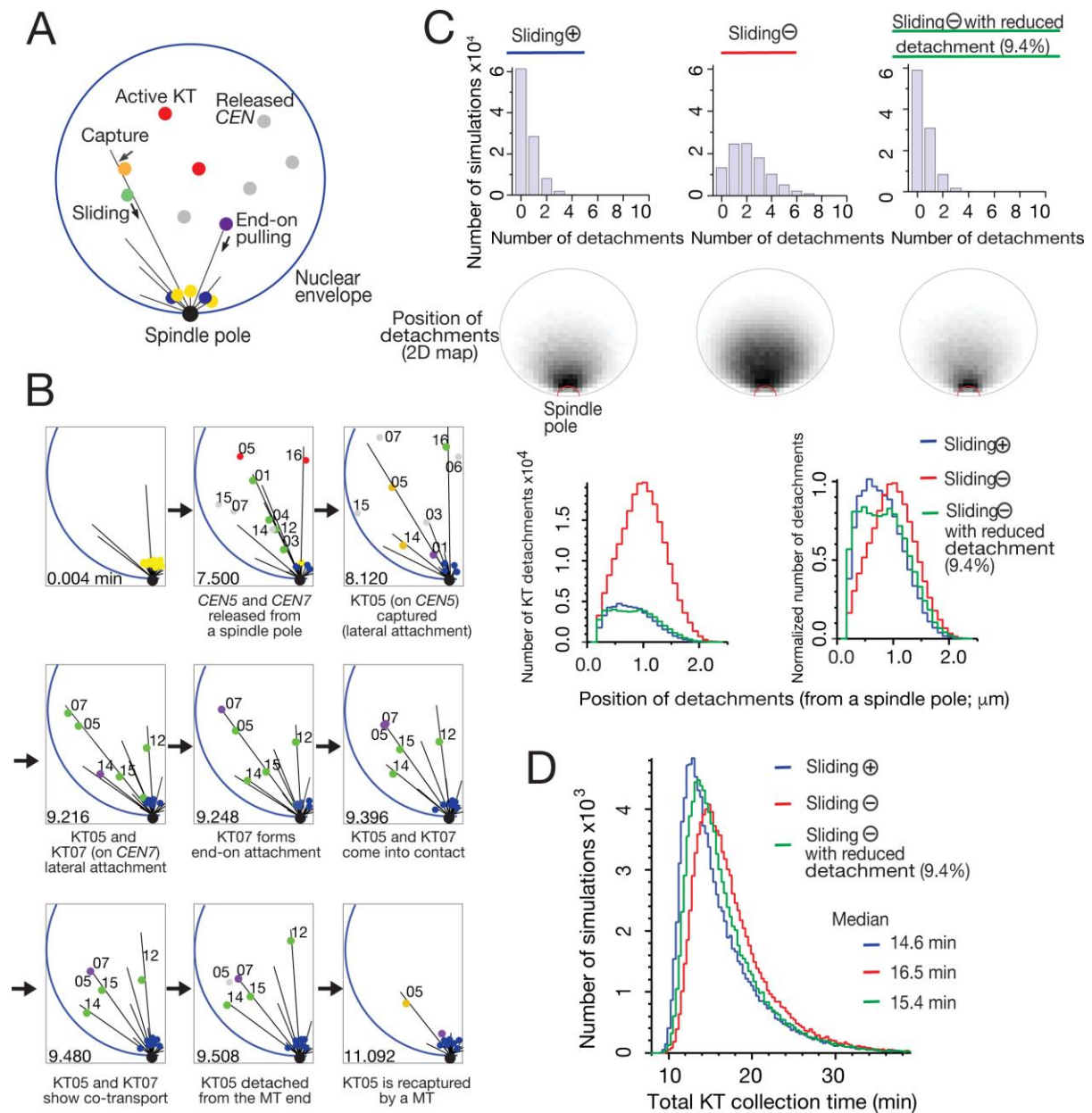
Figure 5. Mathematical simulation shows KT lateral sliding along MTs shortens total KT collection time by delaying and diminishing discernible KT detachments

A) Diagram outlining a computer simulation that recapitulates the initial KT–MT interaction, projected on the X-Z plane (Gandhi et al., 2011). KTs locate in the vicinity of a spindle pole before centromere (*CEN*) DNA replication (yellow dots). Upon *CEN* replication, KTs disassemble, and *CEN*s move away from a pole (gray dots) (Kitamura et al., 2007). KTs are then reassembled (red dots) on *CEN*s, interact with the lateral side of MTs extended from a spindle pole (orange dots) and slide along a MT towards a spindle pole (green dots). KTs are then tethered at the MT end and transported polewards by MT end-on pulling (purple dots). Subsequently they are tethered at the end of short MTs in the vicinity of the pole (blue dots). Representative examples of

computer simulations are shown in Supplemental Movies 6 and 7.

B) Example of KT detachment, after an end-on attached KT coming into contact with a laterally attached KT, in the absence of KT sliding, projected on the X-Z plane. At 9.396 min, an end-on attached KT (KT07; KT on *CEN7*) came into contact with a laterally attached KT (KT05; KT on *CEN5*). After co-transport for a short period, the laterally attached KT05 showed detachment at 9.508 min.

C) Frequency and positions of KT detachments. 100,000 simulations were carried out in each of the following three conditions: the presence (wild-type condition) and absence of sliding, and no sliding with reduced detachments (9.4 % of 'standard' no-sliding condition). In each condition, graph (top) shows the numbers of simulations (y-axis) with the indicated number of KT detachments (x-axis); two-dimensional density maps (middle) show the positions of KT detachments, projected onto the X-Z plane; graph (bottom, left) shows the numbers of KT detachments (y-axis), which happened at the distance from a spindle pole (x-axis), categorized in each bin (0.09 µm); numbers of KT detachments are also shown (bottom, right) after normalization (maximum number was normalized to 1.0 in each condition).

D) Total KT collection time, i.e. time from the first centromere detachment from a spindle pole until the last centromere reaching a pole and forming the end-on attachment, was analyzed in three conditions in C. A total of 100,000 simulations were carried out in each condition. Graph shows the number of simulations (y-axis) with total KT collection time (x-axis), categorized in each bin (0.32 min interval).

Supplemental Figures
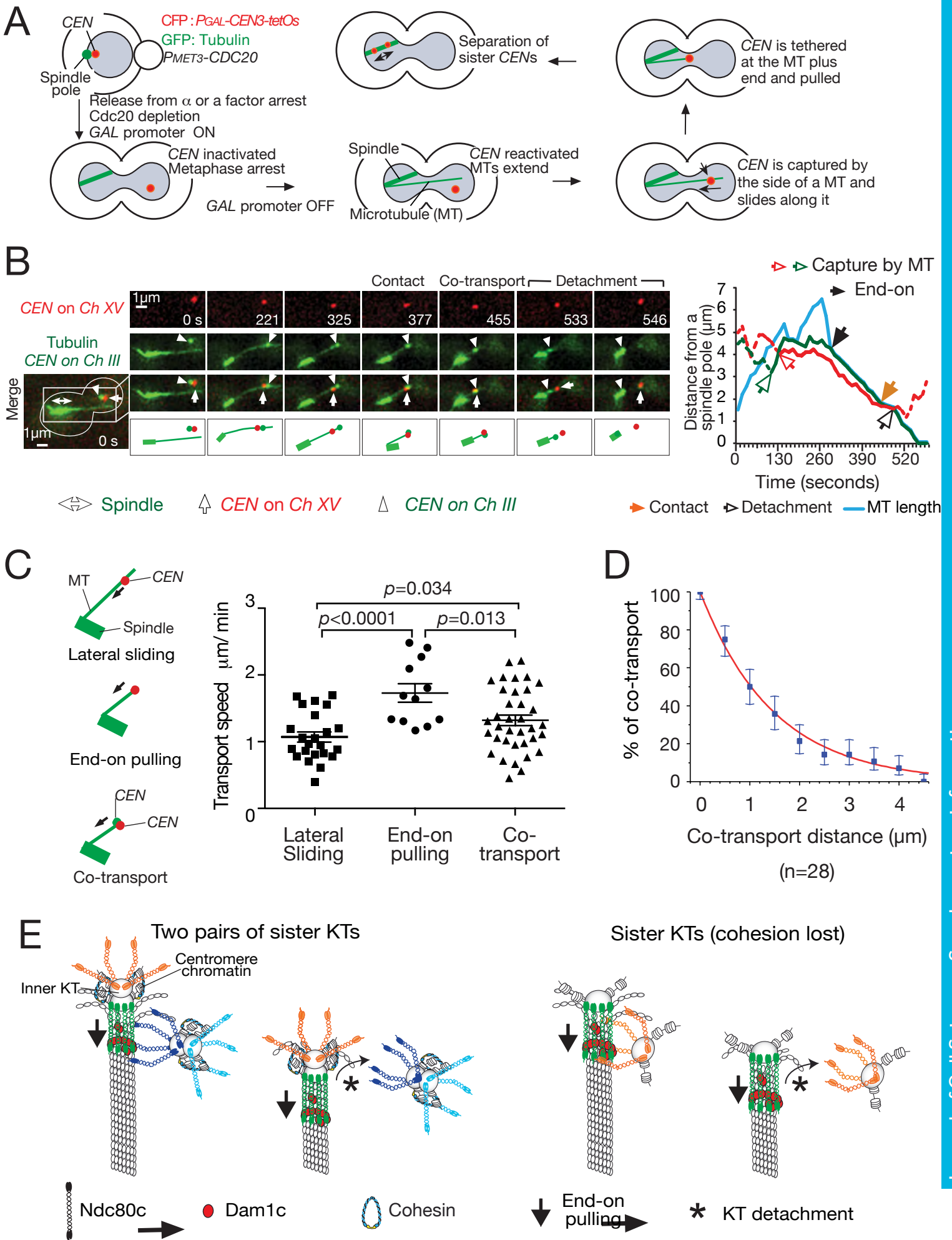
Figure S1. Supplemental Figure associated with Figures 1 and 2

A) Engineered assay system to analyze individual KT–MT interactions with high spatial resolution in budding yeast (Tanaka et al., 2005). CFP: cyan fluorescent protein. GFP: green fluorescent protein.

B) Another representative example (in addition to Figure 1D) where an originally laterally attached KT showed detachment from the MT end after coming into contact with an end-on attached KT. T9717 cells (see Figure 1D) were treated as in Figure 1C. Images and graphs are shown as in Figure 1C. Note that the weak green signal at *CEN* on chromosome XV at 325 s and 546 s likely comes from KT-associated MTs (Kitamura et al., 2010).

C) Diagram on left shows three KT transport modes (lateral sliding, end-on pulling and co-transport). Graph on right shows KT transport speed with the three transport modes. T9717 cells (see Figure 1D) were treated as in Figure 1C. In each mode of transport, the transport speed of P_{GAL}-*CEN3* on chromosome XV (*tetO* fluorescent dot) was measured. Graphs show individual data points and mean ± SEM. The speed of the lateral sliding along a MT was evaluated when *CEN* moved continuously for 1 μm or more in one direction. The sliding speed of P_{GAL}-*CEN3* on chromosome XV was very similar in the presence and absence of P_{GAL}-*CEN3* on chromosome III (*lacO* fluorescent dot) on the lateral side of the same MT.

D) Detachment of *CEN* from the MT end occurs at an approximately constant rate during co-transports of two *CEN*s following their contact (refer to the diagram in Figure 1B). The images collected for Figure 1D were analyzed further. The graph shows how the percentage of co-transports of *CEN*s decreases as the co-transport proceeds and detachment of one *CEN* takes place. The data points in blue show the measured percentage, the error bars represent standard errors of proportions, and a red line shows a regression curve (a simple exponential decay curve). The percentage of remaining co-transports (in which detachment of one *CEN* has not occurred yet) declines approximately following a simple exponential decay curve. This suggests that detachment of one *CEN* happens approximately at a constant rate (per length of a co-transport).

E) Diagrams show models about how an end-on attached KT excludes a laterally attached KT from forming the end-on attachment and causes its detachment from the MT. On the left, two pairs of sister KTs are on one MT. One forms the end-on attachment, while the other interacts with the MT lateral side, close to the MT end, and subsequently detaches from the MT. We speculate that, while one sister KT attaches to the MT end, the other sister is not involved in MT attachment, since one sister KT is sufficient to form 'exclusive' end on attachment (see right; Figure 2). On the right, two sister KTs, which are separate from each other due to a loss of cohesion, interact with one MT. One sister forms the end-on attachment, while the other sister interacts with the MT lateral side (close to the MT end) and subsequently detaches from the MT. The Ndc80 and Dam1 complexes of KTs interact with each other to configure end-on attachment, (Gonen et al., 2012; Kalantzaki et al., 2015; Lampert et al., 2010; Maure et al., 2011; Tien et al., 2010) while the Ndc80, but not the Dam1 complex, are involved in lateral KT–MT interaction (Kalantzaki et al., 2015; Tanaka et al., 2007). The diagrams show speculative configuration of these complexes. The Ndc80 complexes on each sister KT are highlighted in different colors.

A

Lateral sliding

CEN sliding along a MT

Transport speed μm/min (plus value: towards a spindle pole)

| Kar3 | Wild-type | Deleted | Wild-type | Depleted |
| Slk19 | Wild-type | Wild-type | Depleted | Depleted |

B

■ Kar3 Wild-type
▲ Kar3 Depleted
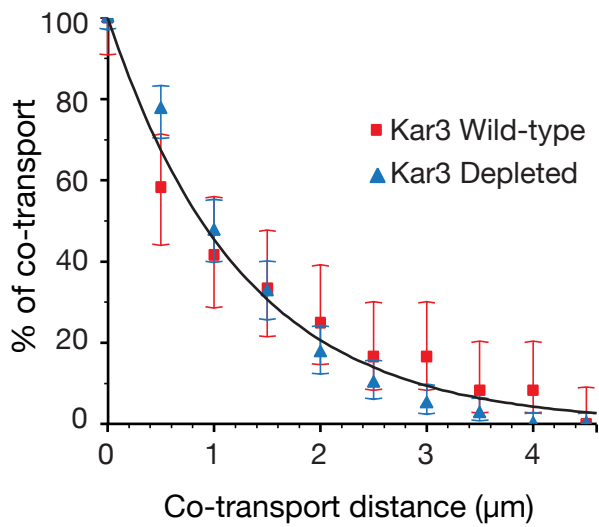
% of co-transport

Co-transport distance (μm)
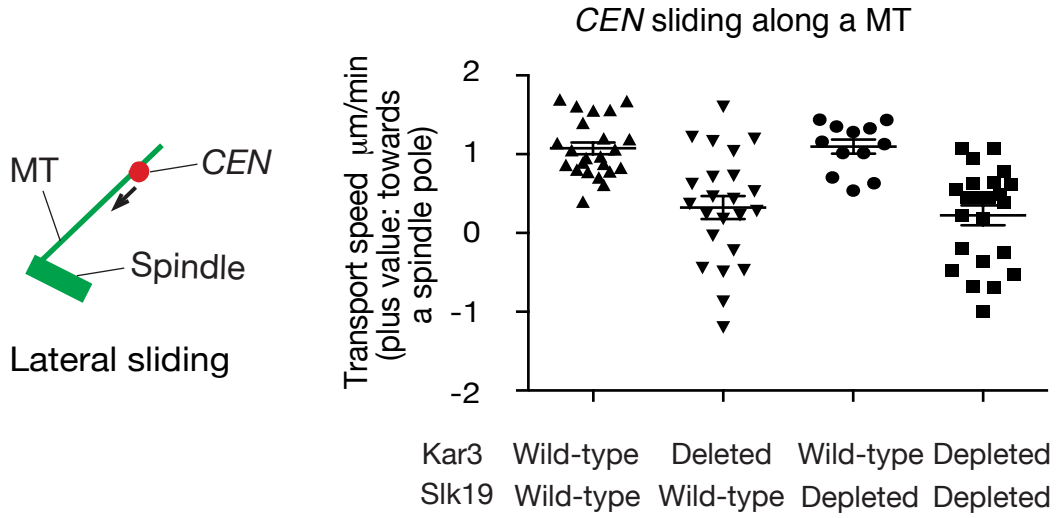
Figure S2. Supplemental Figure associated with Figure 3

A) Kar3 promotes KT sliding along a MT, similarly in the presence and absence of Slk19. To address the effects of KT sliding along a MT on the positions and frequency of KT detachments, we needed to analyze KT behavior in several samples in the presence and absence of Kar3, where two *CEN*s (two pairs of sister *CEN*s), not associated with each other, were caught separately on the MT lateral side. However, contrary to our requirements, two *CEN*s were often associated with each other, prior to the MT interaction after metaphase arrest. Such association was observed after cells were arrested in mitosis (e.g. with nocodazole (Richmond et al., 2013) or Cdc20 depletion), but not observed in physiological conditions. Association between multiple *CEN*s is dependent on Slk19 when cells are arrested in mitosis (Richmond et al., 2013). Therefore, to ensure the two reactivated *CEN*s separate from each other, we depleted Slk19 and compared the behaviors of *CEN*s in Kar3 wild type and Kar3-depleted (or *kar3∆*) cells. *KAR3+* (T9717) and *kar3∆* (T10013) cells with *SLK19+ P_{GAL}-CEN3-tetOs* (replacing *CEN15*) *TetR-3×CFP P_{GAL}-CEN3-lacO* (replacing *CEN3*) *GFP-LacI GFP-TUB1 P_{MET3}-CDC20* were treated as in Figure 1C, and images (CFP and GFP signals) were acquired every 13 sec. Meanwhile, *KAR3+* (T11497) and *kar3-aid* (T11469) cells with *slk19-mini-aid TIR1 P_{GAL}-CEN3-tetOs* (replacing *CEN15*) *TetR-3×CFP P_{GAL}-CEN3-lacO* (replacing *CEN3*) *GFP-LacI-GFP GFP-TUB1 P_{MET3}-CDC20* were treated as in Figure 3A, and images (CFP and GFP signals) were acquired every 18 sec. The speed of the *CEN3-tetOs* motion along a MT was evaluated i) when it moved continuously for 1 µm or more in one direction, or ii) when it was present on a MT lateral side (without reaching a spindle or being converted to end-on attachment) for 1 min or longer. Graphs show individual data points and mean ± SEM. The results suggest that Kar3 facilitates KT sliding along a MT towards a spindle pole, to a similar extent with and without Slk19.

B) Detachment of *CEN* from the MT end occurs at a similar rate in Kar3 wild-type and Kar3-depleted cells, during co-transports of two *CEN*s following their contact (refer to the diagram in Figure 1B). The images collected for Figure 3 were analyzed further. The graph shows how the percentage of co-transports of *CEN*s decreases as the co-transport proceeds and detachment of one *CEN* takes place. The measured percentage is shown for Kar3 wild-type (red squares) and Kar3-depleted (blue triangles) cells and the error bars represent standard errors of proportions. The percentage of remaining co-transports (in which detachment of one *CEN* has not occurred yet) declines similarly between Kar3 wild-type and Kar3-depleted cells, suggesting that the rate of *CEN* detachment (per length of a co-transport) is similar between the two cells. The percentage also declines approximately following a simple exponential decay curve (black line), suggesting that detachment of one *CEN* happens approximately at a constant rate.
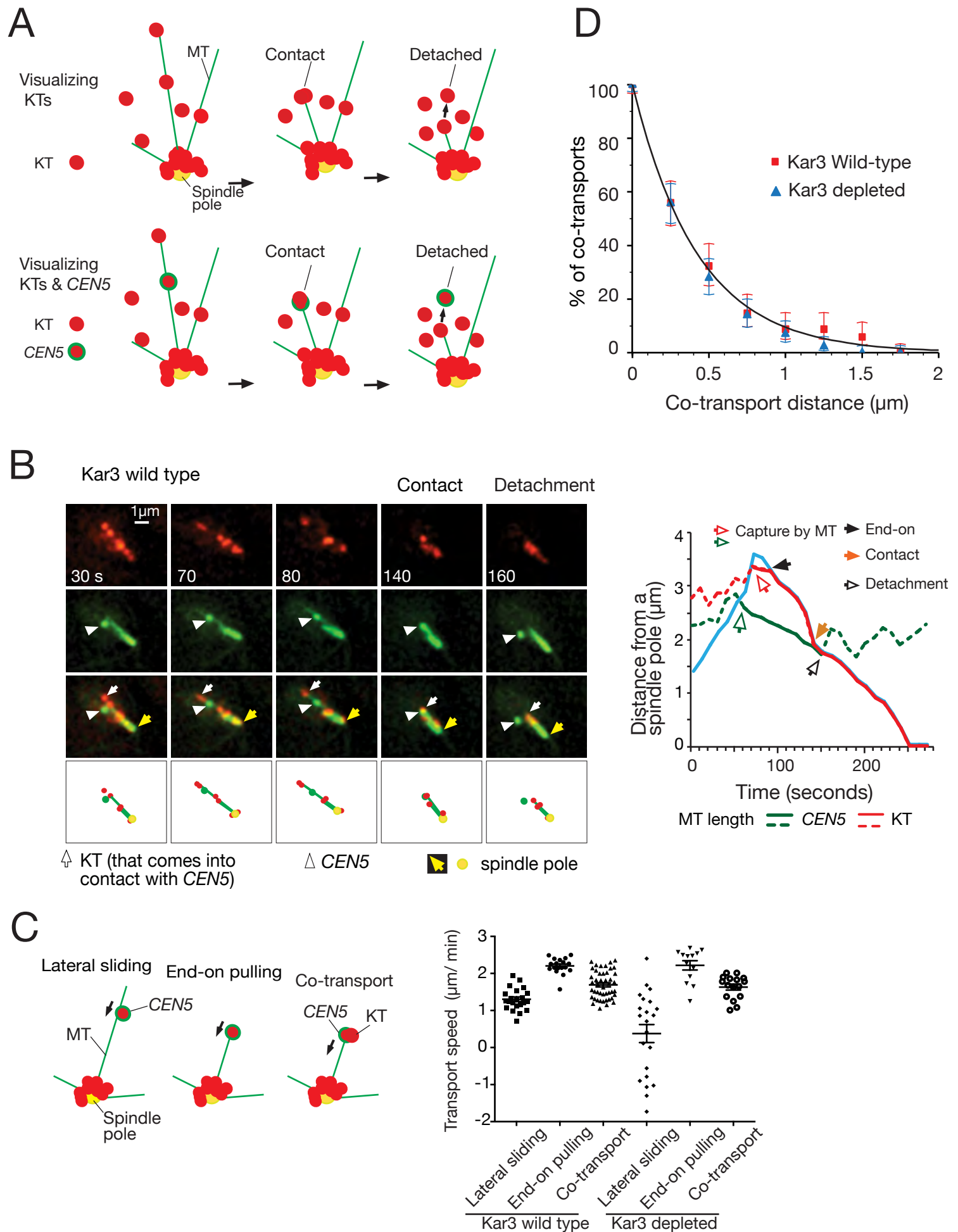
A Visualizing KTs / MT / Contact / Detached / KT / Spindle pole

Visualizing KTs & *CEN5* / Contact / Detached / KT / *CEN5*

B Kar3 wild type / Contact / Detachment

1µm / 30 s / 70 / 80 / 140 / 160

⇧ KT (that comes into contact with *CEN5*)   △ *CEN5*   ◆● spindle pole

C Lateral sliding / End-on pulling / Co-transport / *CEN5* / MT / KT / Spindle pole

D

% of co-transports vs. Co-transport distance (µm)

■ Kar3 Wild-type
▲ Kar3 depleted

Distance from a spindle pole (µm) vs. Time (seconds)

▷ Capture by MT ▶ End-on
▷ Contact
▷ Detachment

MT length   — *CEN5*   — KT

Transport speed (µm/min): Lateral sliding / End-on pulling / Co-transport — Kar3 wild type / Kar3 depleted

Figure S3. Supplemental Figure associated with Figure 4

A) The reason for visualizing one *CEN* and KTs to analyze KT detachments in physiological conditions. To analyze the outcome of two KTs interacting with a single MT (e.g. KT detachment), we initially visualized two *CEN*s in physiological conditions. In contrast to cells arrested in mitosis (see the legend for Figure S2A), two *CEN*s did not associate with each other before they interacted with MTs. However, two *CEN*s rarely interacted with the same MT. Second, we visualized KTs and, in some cases, one KT seemed to detach after a laterally-attached KT came into contact with a KT at the MT end (A, top). However, it was not easy to discern a KT detachment, because it was possible that newly formed KTs were interpreted incorrectly as detached KTs. To overcome this problem, we visualized one *CEN* and KTs, and analyzed the cases where the *CEN* and one KT (on another *CEN*) interacted with, presumably, a single MT (A, bottom; *CEN* closer to a spindle pole and the KT further from it). In this condition, we could clearly discern detachment of the *CEN*.

B) A representative example of *CEN5* detachment (following contact with an end-on attached KT [not on *CEN5*]) in a Kar3 wild-type cell with physiological condition. T11435 cells (see the legend for Figure 4C) were treated and images were acquired as in Figure 4A.

C) The speed of KT end-on pulling, sliding, and co-transport in physiological conditions. T11435 cells (see Figure 4C) were treated, and images were acquired, as in Figure 4C. The speed of *CEN*5 motion in each mode was measured. To measure the co-transport speed, we chose samples where *CEN5* on the MT lateral side came into contact with a KT (on another *CEN*) at the end of, presumably, the same MT. Graphs show individual data points and mean ± SEM.

D) Detachment of *CEN* from the MT end occurs at a similar rate in Kar3 wild-type and Kar3-depleted cells, during co-transports of *CEN5* and a KT (at a different *CEN*) following their contact (refer to the diagram in Figure 4B), in physiological conditions. The images collected for Figure 4 were analyzed further. The graph shows how the percentage of co-transports of *CEN5* and a KT decreases as the co-transport proceeds and detachment of *CEN5* takes place. The measured percentage is shown for Kar3 wild-type (red squares) and Kar3-depleted (blue triangles) cells and the error bars represent standard errors of proportions. The percentage of remaining co-transports (in which detachment of *CEN5* has not occurred yet) declines similarly between Kar3 wild-type and Kar3-depleted cells, suggesting that the rate of *CEN5* detachment (per length of a co-transport) is similar between the two cells. The percentage also declines approximately following a simple exponential decay curve (black line), suggesting that detachment of one *CEN* happens approximately at a constant rate. Note that the rate of KT detachment is higher in physiological conditions (this figure) than in the centromere re-activation assay (Figure S2B). The reason for this difference is unclear. However, the number of molecules of KT components is higher with the centromere-reactivation assay, compared in physiological conditions, when KTs initially interact with MTs (Kitamura et al., 2007). A higher number of KT components (such as the Ndc80 complex) may allow a laterally attached KT to stay in the vicinity of the MT end (which is occupied by an end-on attached KT) for a longer period.
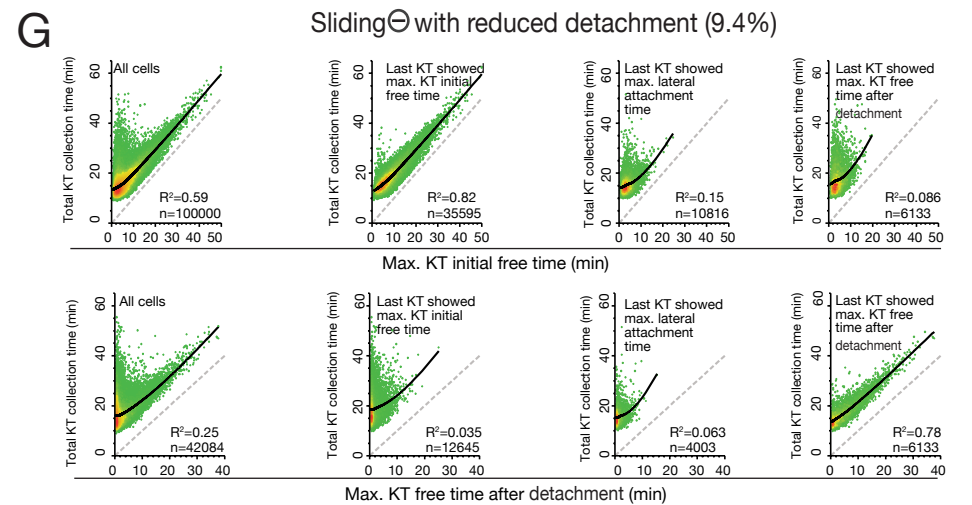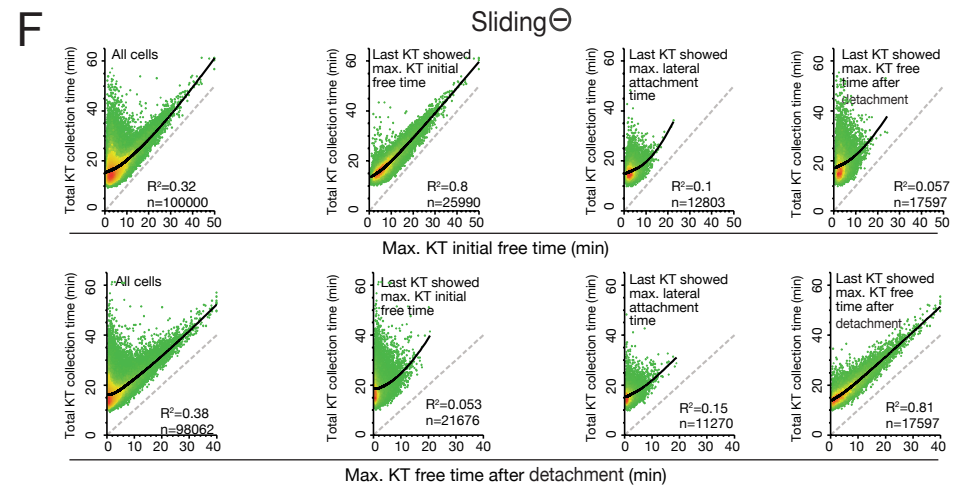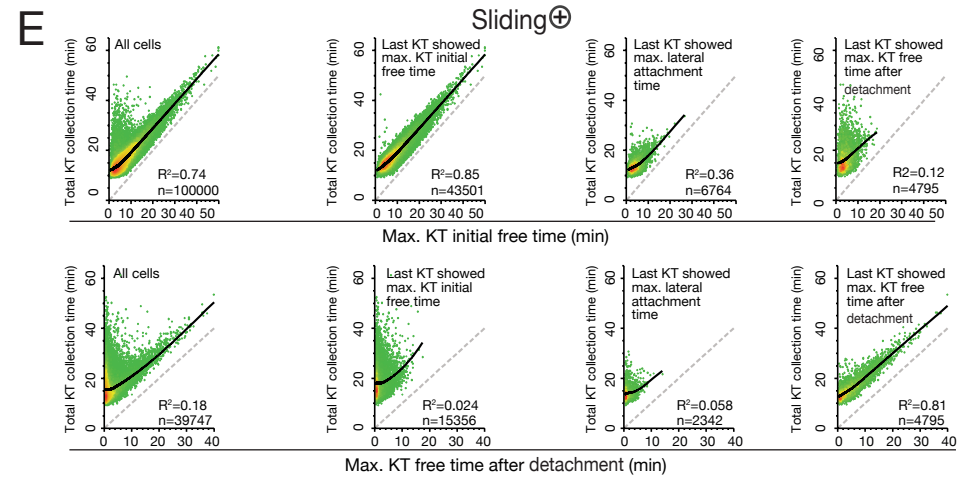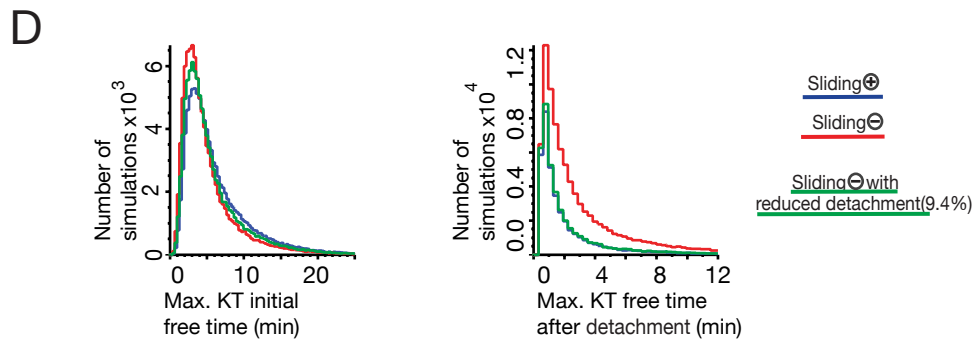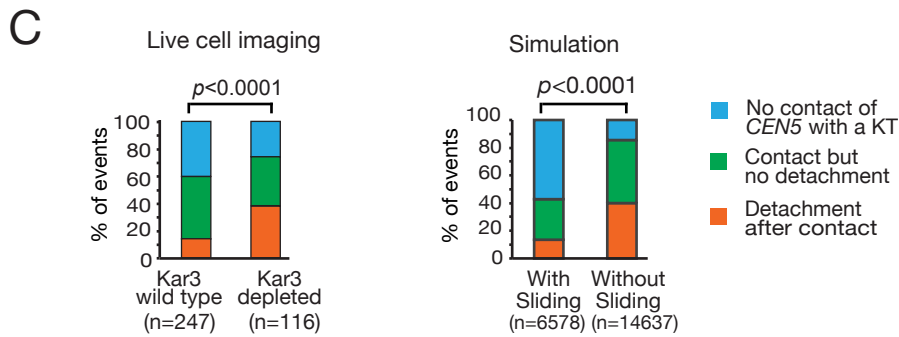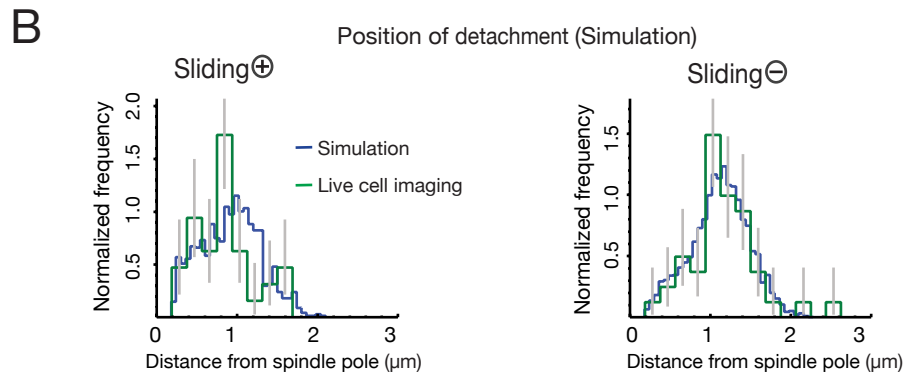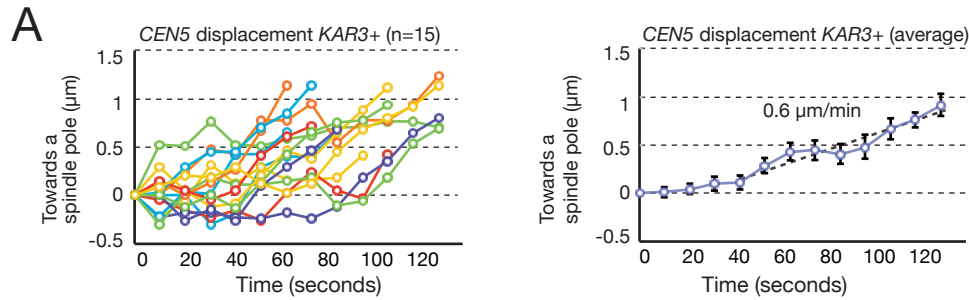
Figure S4. Supplemental Figure associated with Figure 5

A) Quantifying the average speed of KT displacement along a MT. Cells (T7470) with *CEN5-tetOs TetR-3×CFP GFP-TUB1* was treated and images were acquired as in Figure 4A except that NAA was not added. Graph on left shows the position of *CEN5* for a short period, during which it was on the MT lateral side but not at the MT plus end. Each line represents a time course trajectory of *CEN5* along a MT in an individual cell. On x-axis and y-axis, zero represents the time and position (along a MT), respectively, of the initial *CEN5* capture by the MT lateral side. Plus values on y-axis represent *CEN5* displacement towards a spindle pole. Graph on right shows the displacement of *CEN5* from its original position along a MT, averaged among different cells shown in the left graph, while *CEN5* is on the MT lateral side. Error bars show standard errors of means. We interpret that *CEN5* motion is relatively slow during 0–40 seconds, compared with a later period. We reason that, in some cells, *CEN5* may not be physically on a MT during this period (note that an overlap of a *CEN5* signal with a MT signal does not necessarily mean physical *CEN5*-MT interaction because of limited spatial resolution in light microscopy). Thus we analyzed the average *CEN5* motion during 40–120 seconds, and estimated that the average speed of *CEN5* displacement was 0.6 µm/min towards a spindle pole along a MT. Note that the speed of KT lateral sliding in Figures S1C, S2A and S3C shows the speed when KT was moving continuously (see details in legends of Figures S1C, S2A and S3C). However a KT on the MT lateral side may also show short pausing and a brief motion away from a pole (see graph on left, this figure). Graph on right of this figure shows the average speed of KT displacement, including short pausing and brief motion away from a spindle pole. Therefore the average KT displacement speed measured in this figure is smaller than the average KT sliding speed in Figure S3C.

B) Positions of *CEN5* detachments distribute similarly in live-cell imaging and in simulation. Left graph shows *CEN5* detachment positions with KT sliding (*KAR3*+ wild-type in live-cell imaging), while right graph shows those without KT sliding (Kar3 depletion in live cell imaging). In both graphs, green line shows results from live cell imaging (Figure 4C, right) and blue line shows results from simulation. X-axis shows distance of *CEN5* detachments from a spindle pole (categorized in bins; 0.1875 and 0.06 µm interval for green and blue, respectively), while y axis- shows normalized frequency. Gray bars show standard errors of proportion in live-cell imaging results.

C) Frequency of *CEN5* detachments (orange) is similar in live-cell imaging (left) and in simulation (right). Graphs show how *CEN5* reaches a spindle pole or shows detachment, after *CEN5* and another KT are caught on the same MT. For live-cell imaging data, graphs in Figure 4D are copied here for comparison. Three categories are explained in Figure 4D legend (refer to Figure 4B). Frequency of the three categories was also obtained in 100,000 simulations with and without KT sliding. Note that the sample number (n number) is larger with Kar3 wild-type than with Kar3 depletion in live-cell imaging whereas it is larger without sliding than with sliding in simulation; this is because a larger number of Kar3 wild-type cells were observed in live-cell imaging in order to analyze a sufficient number of detachments with Kar3 wild-type.

D) Maximum KT initial free time and maximum KT free time after detachment. We have analyzed a maximum time (among 16 KTs) of KT being active but left unattached to a MT after moving away from a spindle pole following centromere replication (Max. KT initial free time; left) and a maximum time (among all detachment events in each simulation) of KT being left unattached to a MT following detachment after contact of two KTs on the same MT (Max. KT free time after detachment; right), in the three conditions analyzed in Figure 5C and D. The graphs show the numbers of simulations (y-axis) with these maximum times (x-axis), categorized in each bin (0.32 min interval).

E–G) The behavior of the last KT in individual simulations has been analyzed. How do

the diminished detachments, following contact of two KTs on the same MT, shorten the total KT collection time? In other words, how do more frequent KT detachments lead to a longer total KT collection time? To address this, we investigated the last KT that reached to the vicinity of a spindle pole (and formed end-on attachment to a short MT there), as it determines the total KT collection time in each simulation. More specifically, we addressed whether the last KT spent a long time in the following process: 1) being active but left unattached to a MT after moving away from a spindle pole following centromere replication (KT initial free time); 2) being left unattached to a MT following an detachment after contact of two KTs (KT free time after detachment); and/or 3) being on the MT lateral side (lateral attachment time). We compared the amount of time spent by each KT in 1), 2) and 3) among all KTs or among all relevant events in each simulation, and identified the KT that spent the longest time in each process. Then individual simulations were categorized into three subgroups, in which the last KT was identical to the KT that spent the longest time in 1), 2) and 3); i.e. the last KT showed 'max. KT initial free time', 'max. KT free time after detachment' and 'max. lateral attachment time' (if a simulation belonged to two or three subgroups, it was not included in further analyses). In each subgroup, we plotted total KT collection time against 'max KT initial free time' and 'max KT free time after detachment' in individual simulations (if no KT showed detachment in a simulation, that simulation was not included in plotting against 'max KT free time after detachment'). This analysis was carried out with the three conditions analyzed in Figure 5C and D, and the results are shown in A, B and C. In each graph, red and green represents high and low density of samples, respectively; a dashed line shows the line x=y; a black line represents a loess curve, which shows locally weighted polynomial regression that smooths y values against a local change along x-axis; a R squared is a coefficient of determination showing how well data points follow the loess curve. We interpret that, when total KT collection time showed high correlation with 'max. KT initial free time' or 'max. KT free time after detachment', the total KT collection time was determined by such maximum time. When KT sliding was present (A), the majority of the last KT showed 'max. KT initial free time', determining total KT collection time. When KT sliding was switched off (B), there was a substantial increase in the population (from 4795 to 17597), in which the last KT experienced 'max. KT free time after detachment', determining total KT collection time (B, bottom right). When detachment frequency was reduced to 9.4 % in the absence of KT sliding (C), this population was reduced to a level (6133) close to that with KT sliding (4795). Overall these results suggest that, after frequent KT detachments (following contact of two KTs) in the absence of KT sliding, some detached KTs spent a long time before being recaptured by a MT and became the last KT reaching a spindle pole, which prolonged total KT collection time.

Table S1. Yeast strains used in this study

The table shows genotypes of yeast strains used in this study. All strains used in this study are derivatives of *Saccharomyces cerevisiae* W303 (K699 and K700 from Kim Nasmyth lab).

Strain	Genotype
T6519	*MATalpha P_{GAL}-CEN3-lacOs::URA3 his3::GFP-lacI::HIS3 cen15Δ::P_{GAL}-CEN3-tetOs::URA3 ade1::TetR-3xCFP::hphMX trp1::P_{TUB1}YFP-TUB1::TRP1 P_{MET3}-CDC20::TRP1*
T7470	*MATa CEN5::tetOs::HIS3 leu2::tetR-3xECFP::HPH1 ura3::P_{TUB1}-GFP-TUB1::URA3*
T9717	*MATa P_{GAL}-CEN3-lacOs::URA3 his3::GFP-lacI::HIS3 cen15Δ::P_{GAL}-CEN3-tetOs::URA3 ade1::TetR-3xCFP::hphMX trp1::GFP-TUB1::TRP1 P_{MET3}-CDC20::TRP1*
T10013	*MATa kar3Δ::kanMX P_{GAL}-CEN3-lacOs::URA3 his3::GFP-lacI::HIS3 cen15Δ::P_{GAL}-CEN3-tetOs::URA3 ade1::TetR-3xCFP::hphMX trp1::GFP-TUB1::TRP1 P_{MET3}-CDC20::TRP1*
T10546	*MATa cen15Δ::P_{GAL}-CEN3-tetOs::URA3 ade1::TetR-3xCFP::hphMX his3::GFP-TUB1::HIS3 RPL13A-2xFKBP12::TRP1 TOR1-1 fpr1Δ::natMX4 P_{MET3}-CDC20::TRP1*
T11434	*MATa KAR3-aid::natNT2 ura3::P_{ADH1}-TIR1::URA3 MTW1-4xmCherry::natMX6 CEN5::tetOs::HIS3 leu2::tetR-GFP::LEU2 Ndc80-4mCherry::NatMX6 his3::P_{TUB1}-GFP-TUB1::HIS3*
T11435	*MATalpha ura3::P_{ADH1}-TIR1::URA3 MTW1-4xmCherry::natMX6 Ndc80-4mCherry::natMX6 CEN5::tetOs::HIS3 leu2::tetR-GFP::LEU2 his3::P_{TUB1}-GFP-TUB1::HIS3*
T11469	*MATa KAR3-aid::natNT2 SLK19-aid::kanMX ura3::P_{ADH1}-TIR1::URA3 P_{GAL}-CEN3-lacOs::URA3 his3::GFP-lacI::HIS3 cen15Δ::P_{GAL}-CEN3-tetOs::URA3 ade1::TetR-3xCFP::hphMX trp1::GFP-TUB1::TRP1 P_{MET3}-CDC20::TRP1*
T11497	*MATa SLK19-aid::kanMX ura3::P_{ADH1}-TIR1::URA3 P_{GAL}-CEN3-lacOs::URA3 his3::GFP-lacI::HIS3 cen15Δ::P_{GAL}-CEN3-tetOs::URA3 ade1::TetR-3xCFP::hphMX trp1::GFP-TUB1::TRP1 P_{MET3}-CDC20::TRP1*
T11941	*MATa cen15Δ::P_{GAL}-CEN3-tetOs::URA3 ade1::TetR-3xCFP::hphMX his3::GFP-TUB1::HIS3 leu2::GFP-TUB1::LEU2 SCC1-FRB::kanMX6 RPL13A-2xFKBP12::TRP1 TOR1-1 fpr1Δ::natMX4 P_{MET3}-CDC20::TRP1*

Table S2. Parameters and their values used in simulation

The table shows parameters and their values used in the computer simulation shown in Figures 5 and S4.

Parameter	Symbol	Value	Source of the value
Time step	Δt	0.001 min	A reasonably small value was chosen
Radius of the nucleus	R_{nuc}	1.25 µm	Natsume et al, 2013 (visualization of the nuclear envelope)
Initial MT number	n_{MT}	5	Based on Fig S1E etc. Kitamura et al., 2010
Exclusion radius	r_{ex}	0.2 µm	Based on Fig S1E etc. Kitamura et al., 2010
MT growth speed	v_{gro}	1.5 µm min^{-1}	Fig 3b, Tanaka et al. 2005
MT shrinkage speed	v_{shr}	2.8 µm min^{-1}	Fig 3b, Tanaka et al. 2005
MT catastrophe rate	K_{cat}	0.6 min^{-1}	Gandhi et al, 2011
MT nucleation rate	K_{nuc}	1 min^{-1}	Based on Fig S1E etc. Kitamura et al., 2010
MT beaming factor	β	0.7	Based on Fig S1E etc. Kitamura et al., 2010
MT angular diffusion coefficient	D_{MT}	0.03 rad^2 min^{-1}	Based on Kalinina et al 2013
Diffusion coefficient	D	0.1 µm^2 min^{-1}	Fig S1, Kitamura et al., 2007
KT activation delay	t_{del}	2 min	Gandhi et al, 2011
KT lateral displacement speed	v_{lat}	0.6 µm min^{-1}	This study
KT lateral diffusion coefficient	D_{lat}	0.1 µm^2 min^{-1}	Fig 3, Tanaka et al. 2007
KT detachment rate	K_{evi}	4.8 µm^{-1}	This study
KT end-on pulling speed	v_{pul}	1.7 µm min^{-1}	Fig 2D, Tanaka et al. 2007 & Fig 7C, Kitamura et al. 2007
KT slow end-on pulling speed	v_{spul}	0.35 µm min^{-1}	Gandhi et al., 2011
KT co-transport speed	v_{tran}	1.4 µm min^{-1}	This study
KT rescue delay	t_d	8 sec	Gandhi et al., 2011
Stu2 sending rate	K_{stu2}	0.1 min^{-1}	Gandhi et al., 2011
Stu2 speed	v_{stu2}	2.1 µm min^{-1}	Fig S9, Tanaka et al. 2005 & Gandhi et al., 2011
KT capture radius	R_{KT}	0.4 µm	Fig 6A, S6A Kitamura et al., 2010
KT capture speed	v_{cap}	5 µm min^{-1}	Fig S1C, Kitamura et al., 2010
Probability of MT rescue at the KT	P_{res}	0.6	Fig 4B, Tanaka et al., 2007

Supplemental Movies
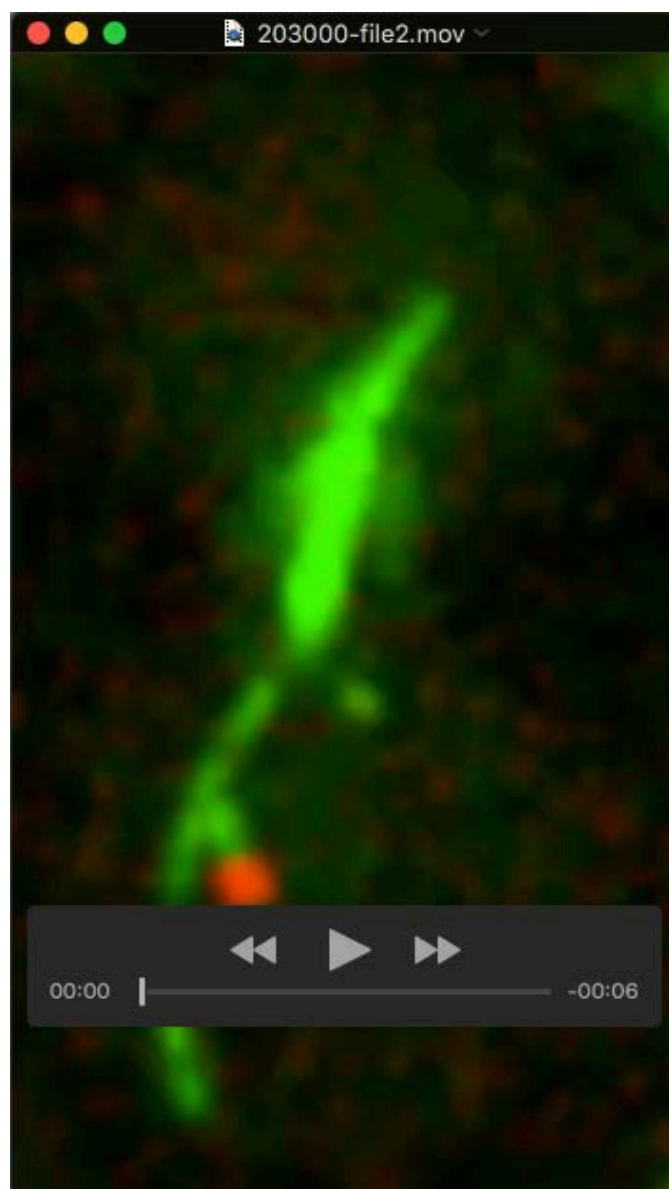
Movie 1. A representative example is shown in which two *CEN*s (two pairs of sister *CEN*s) showed lateral sliding along a single MT (associated with Figure 1C). The procedure of the experiment is explained in the legend for Figure 1C. Green shows the spindle, MTs and *CEN* on chromosome *III* while red shows *CEN* on chromosome *XV*. The interval of frames is 20 sec, and 5 frames are shown per second in the movie.
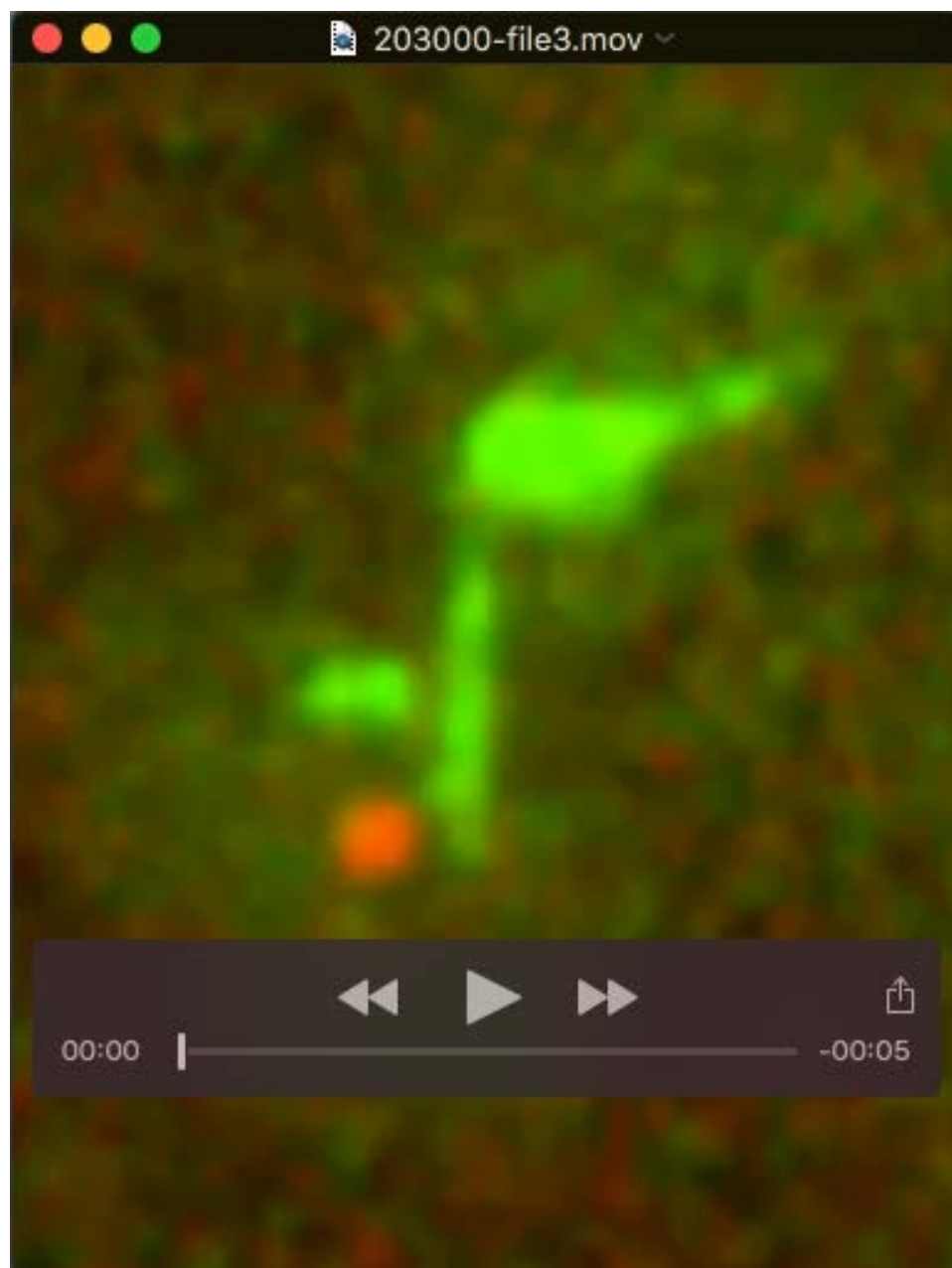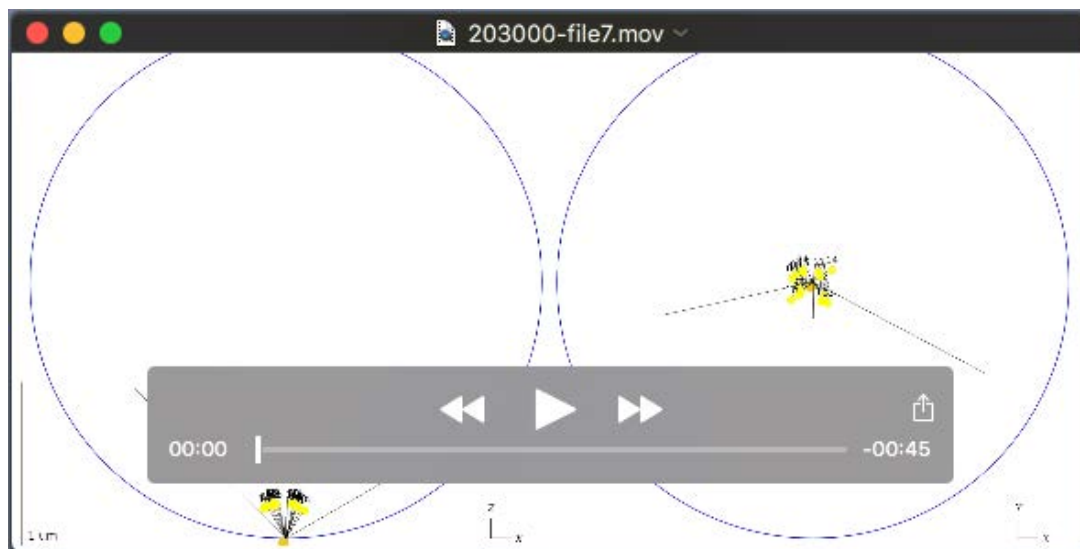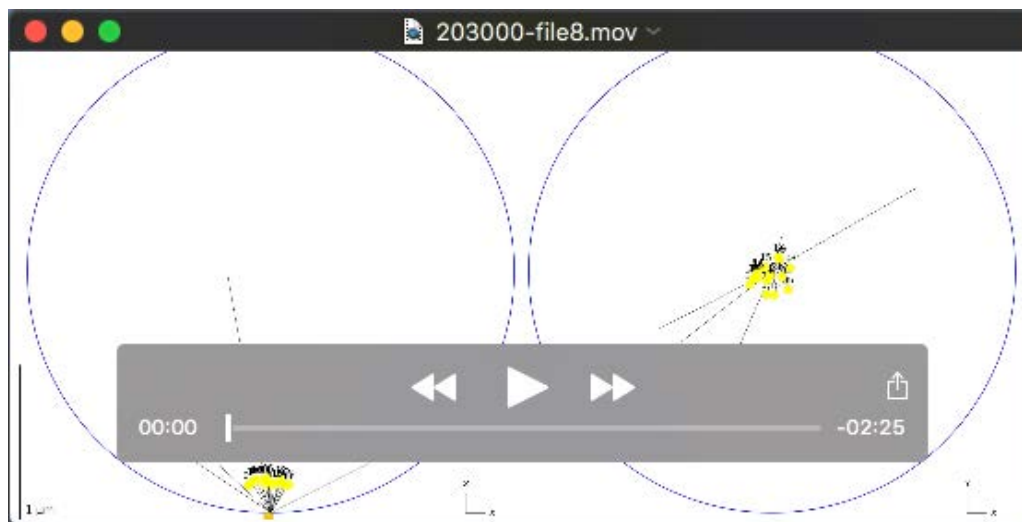
Movie 2. A representative example is shown in which a laterally attached *CEN* showed detachment after coming into contact with an end-on attached *CEN* (associated with Figure 1D). The procedure of the experiment is explained in the legend for Figure 1D. Green shows the spindle, MTs and *CEN* on chromosome *III* while red shows *CEN* on chromosome *XV*. The interval of frames is 13 sec, and 5 frames are shown per second in the movie.
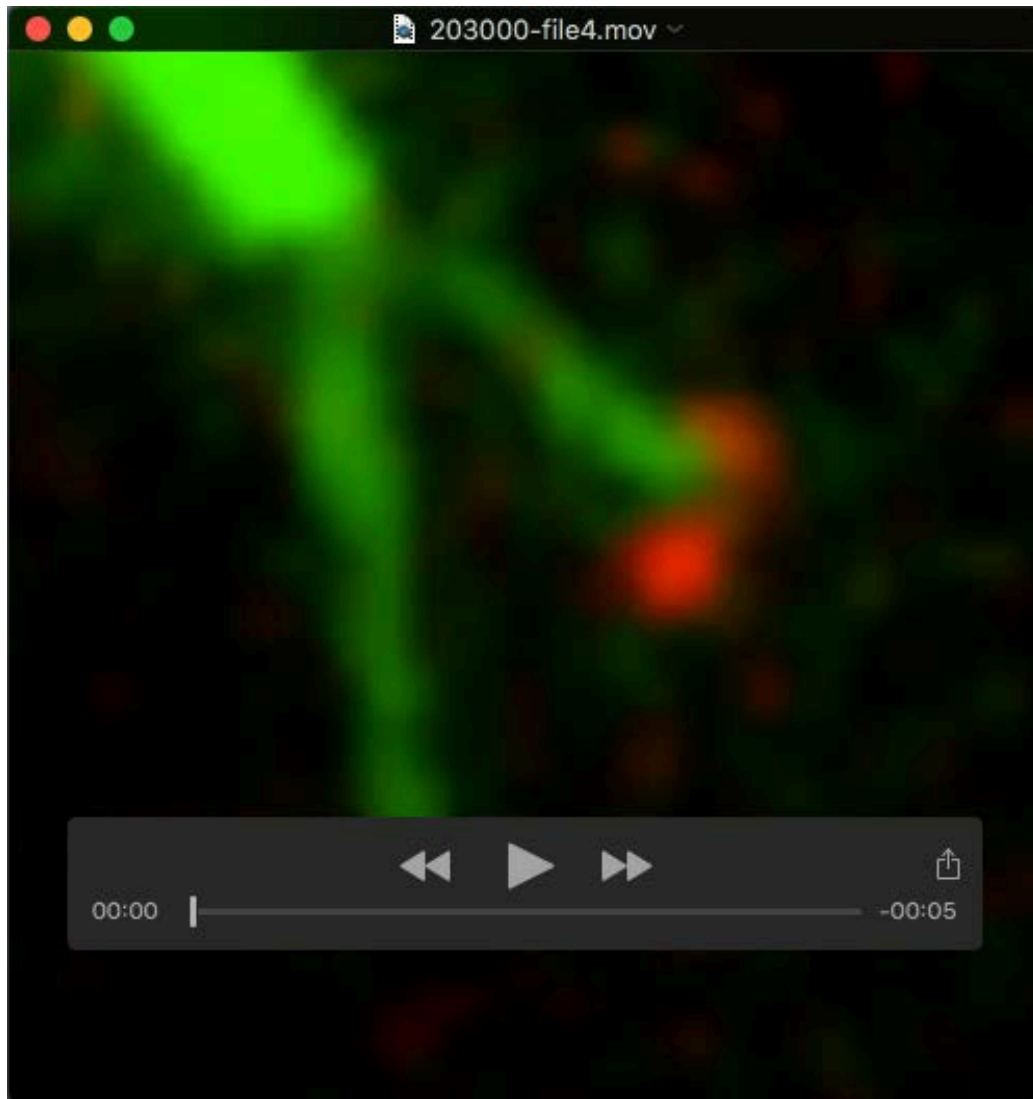
Movie 3. A representative example is shown in which sister *CEN*s interact with a single MT after their cohesion is lost (associated with Figure 2B). The procedure of the experiment is explained in the legend for Figure 2B. Green shows the spindle and MTs while red shows *CEN* on chromosome *XV*. The interval of frames is 10 sec, and 5 frames are shown per second in the movie.
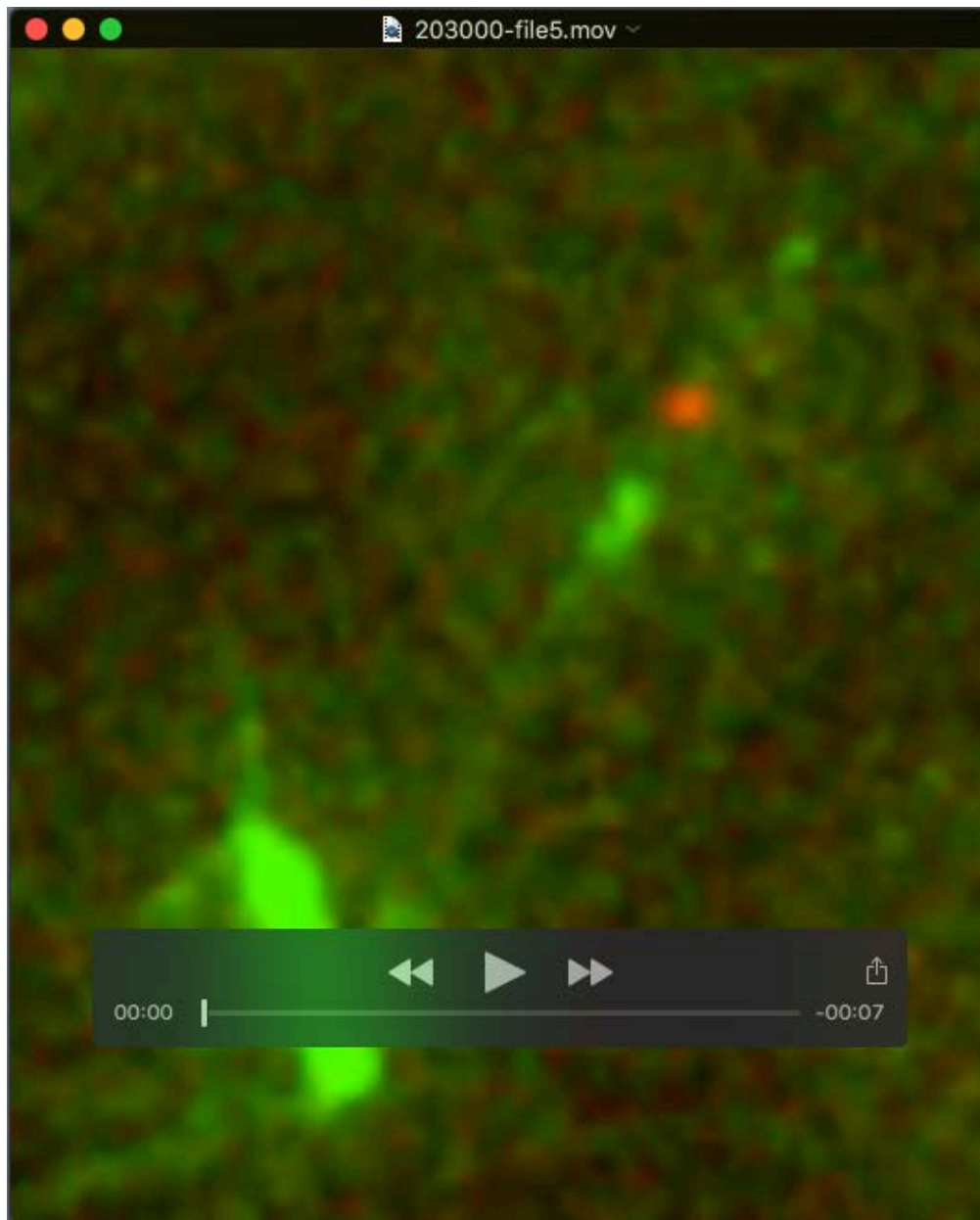
Movie 4. A representative example of a Kar3-depleted cell in which a laterally attached *CEN* showed detachment after coming into contact with an end-on attached *CEN* (associated with Figure 3A). The procedure of the experiment is explained in the legend for Figure 3A. Green shows the spindle, MTs and *CEN* on chromosome *III* while red shows *CEN* on chromosome *XV*. The interval of frames is 18 sec, and 5 frames are shown per second in the movie.

Movie 5. A representative example of *CEN* detachment is shown in physiological condition (associated with Figure 4A). The procedure of the experiment is explained in the legend for Figure 4A. Green shows the spindle, MTs and *CEN5* while red shows KTs. The interval of frames is 10 sec, and 5 frames are shown per second in the movie. Note that, after showing detachment at 210 s, *CEN5* was out of focus during 230-310 s, during which *CEN5* distance from a spindle pole was measured using out-of-focus *CEN5* signals.

Movie 6. A representative example of computer simulation is shown with KT sliding (normal condition, i.e. with KT sliding; associated with Figure 5). Three-dimensional simulations are projected into X-Z and X-Y planes. KTs (dots) are colored as in Figure 5A. MT extension following KT-dependent rescue is shown in a dashed line (Gandhi et al., 2011). A gray line, which connects a KT (dot) to a MT extending from a spindle pole (black line), represents a KT-derived MT that facilitates KT loading onto a MT extending from a spindle pole (Kitamura et al., 2010).

Movie 7. A representative example of computer simulation is shown without KT sliding (associated with Figure 5B). Three-dimensional simulations are projected into X-Z and X-Y planes. KTs (dots) are colored as in Figure 5A. MT extension following KT-dependent rescue is shown in a dashed line (Gandhi et al., 2011). A gray line, which connects a KT (dot) to a MT extending from a spindle pole (black line), represents a KT-derived MT that facilitates KT loading onto a MT extending from a spindle pole (Kitamura et al., 2010).